NeuroImage 141 (2016) 88–107

Contents lists available at ScienceDirect

NeuroImage

journal homepage: www.elsevier.com/locate/ynimg

Transcranial alternating current stimulation modulates spontaneous low frequency fluctuations as measured with fMRI

Yuranny Cabral-Calderin [a,b,*,1], Kathleen A. Williams [a,1], Alexander Opitz [c,d], Peter Dechent [a], Melanie Wilke [a,b,e]

[a] Department of Cognitive Neurology, University Medical Center, Georg-August University Goettingen, Robert-Koch-Str. 40, Goettingen 37075, Germany
[b] German Primate Center, Leibniz Institute for Primate Research, Kellnerweg 4, Goettingen 37077, Germany
[c] Center for Biomedical Imaging and Neuromodulation, Nathan Kline Institute for Psychiatric Research, Orangeburg, NY 10962, USA
[d] Center for the Developing Brain, Child Mind Institute, New York, NY 10022, USA
[e] DFG Center for Nanoscale Microscopy & Molecular Physiology of the Brain (CNMPB), Germany

ARTICLE INFO

Article history:
Received 31 May 2016
Accepted 2 July 2016
Available online 5 July 2016

Keywords:
tACS
Brain stimulation
fMRI
Oscillations
Entrainment
fALFF/ALFF
Intrinsic functional connectivity
Resting state
Cross-frequency coupling

ABSTRACT

Transcranial alternating current stimulation (tACS) is a promising tool for modulating brain oscillations. Combining tACS with functional magnetic resonance imaging (fMRI), we recently showed that tACS applied over the occipital cortex did not exert its strongest effect on regions below the electrodes, but mainly on more distant fronto-parietal regions. Theoretically, this effect could be explained by tACS-induced modulation of functional connectivity between directly stimulated areas and more distant but anatomically and functionally connected regions. In the present study, we aimed to characterize the effect of tACS on low frequency fMRI signal fluctuations. We employed simultaneous fMRI-tACS in 20 subjects during resting state (eyes open with central fixation for ~8 min). Subjects received tACS at different frequencies (10, 16, 40 Hz) and with different electrode montages (Cz-Oz, P5–P6) previously used in behavioral studies. Electric field simulations showed that tACS over Cz-Oz directly stimulates occipital cortex, while tACS over P5–P6 primarily targets parietal cortices. Group-level simulation-based functional connectivity maps for Cz-Oz and P5–P6 resembled the visual and fronto-parietal control resting-state networks, respectively. The effects of tACS were frequency and partly electrode montage dependent. In regions where frequency-dependent effects of tACS were observed, 10 and 40 Hz tACS generally induced opposite effects. Most tACS effects on functional connectivity were observed between, as opposed to within, resting-state networks. The left fronto-parietal control network showed the most extensive frequency-dependent modulation in functional connectivity, mainly with occipito-parietal regions, where 10 Hz tACS increased and 40 Hz tACS decreased correlation values. Taken together, our results show that tACS modulates local spontaneous low frequency fluctuations and their correlations with more distant regions, which should be taken into account when interpreting tACS effects on brain function.

Introduction

Transcranial alternating current stimulation (tACS) is a non-invasive brain stimulation technique that has proven to be effective in modulating brain oscillations (Ali et al., 2013; Helfrich et al., 2014a; Ozen et al., 2010; Zaehle et al., 2010; Reato et al., 2013). A growing body of literature exists documenting frequency-dependent effects of tACS on different brain functions in health (Cabral-Calderin et al., 2015; Feurra et al., 2013, 2011a; Helfrich et al., 2014b; Joundi et al., 2012; Kanai et al., 2008; Kar and Krekelberg, 2014; Laczo et al., 2012; Polania et al., 2012; Santarnecchi et al., 2013; Wach et al., 2013; Wang et al., 2015) and disease (Brittain et al., 2013; Fedorov et al., 2010). For instance, effects of tACS on visual perception have been reported when tACS was applied over occipital and parietal cortices at alpha or gamma frequencies (Helfrich et al., 2014a; Cabral-Calderin et al., 2015; Laczo et al., 2012; Wang et al., 2015). Although these effects have been mainly attributed to increasing the power or synchrony of alpha/gamma oscillations in occipito-parietal areas, recent studies indicate that underlying mechanisms of tACS effects are far more complicated. With the exception of a few studies combining tACS with electroencephalographic (EEG) recordings (Helfrich et al., 2014a; Zaehle et al., 2010) or functional magnetic resonance imaging (fMRI) (Alekseichuk et al., 2015; Cabral-Calderin et al., 2016; Vosskuhl et al., 2015), most of our knowledge about tACS is derived from behavioral studies. Technical challenges inherent to concurrent measurements of brain activity when applying tACS, such as artifacts in EEG signals or the need for specialized

* Corresponding author at: Department of Cognitive Neurology, University Medical Center, Robert-Koch-Str. 40, Goettingen 37075, Germany.
E-mail address: yurany.cabral-calderin@med.uni-goettingen.de (Y. Cabral-Calderin).
[1] Shared first author.

http://dx.doi.org/10.1016/j.neuroimage.2016.07.005
1053-8119/

MRI-safe equipment, leave only several published studies of combined brain imaging and tACS, making it difficult to interpret the behavioral results in terms of the underlying brain activity (Zaehle et al., 2010; Helfrich et al., 2014b; Alekseichuk et al., 2015; Cabral-Calderin et al., 2016; Vosskuhl et al., 2015; Witkowski et al., 2015; Neuling et al., 2015).

In a recent study combining tACS with fMRI (Cabral-Calderin et al., 2016) we showed that the effect of tACS on brain activity, as inferred from the blood-oxygenation-level-dependent (BOLD) signal, is rather complex and cannot entirely be predicted based on electrode positions alone. In general, the effects of tACS over Cz-Oz were frequency-, region-, and task-dependent. Specifically, BOLD activity changes were stronger with lower tACS frequencies; that is, alpha (10 Hz) and beta (16 Hz) frequencies were more effective than gamma (60, 80 Hz). Additionally, effects were mainly observed in regions not activated by the task and that were distant from the electrodes (i.e., fronto-parietal but not occipital regions) (Cabral-Calderin et al., 2016). The fact that the above-mentioned study reported tACS effects mainly in areas distant from the electrodes (i.e., fronto-parietal) could indicate that the effects of tACS are transmitted from directly stimulated brain regions (i.e., occipital) to more distant but anatomically and functionally connected regions. In fact, it has been proposed that the effects of phase entrainment (a possible mechanism of tACS) in a given brain area may propagate through a larger network due to inter-regional phase locking (Canolty and Knight, 2010). It is thus reasonable to assume that tACS also interferes with the dynamics of brain networks. A recent study combining tACS (applied over occipito-parietal areas) with EEG has reported tACS-induced modulation of interhemispheric functional connectivity in occipito-parietal cortices in a phase-specific manner (Helfrich et al., 2014b). The authors reported that in-phase tACS in the gamma range (40 Hz) enhanced interhemispheric synchrony while anti-phase tACS impaired it, providing evidence of the possibility of modifying functional coupling between brain regions with tACS.

The dynamics of intrinsically functionally connected networks have been largely studied with resting-state fMRI (rs-fMRI), in which subjects are not engaged in an active task (e.g., awake with eyes closed or eyes open, with or without eye fixation (Van Dijk et al., 2010)). Over the last two decades many studies have documented the presence of resting-state networks (RSNs) arising from regionally distributed but temporally correlated low frequency BOLD signal fluctuations (<0.1 Hz) in the resting brain (Fox et al., 2005; Fox and Raichle, 2007; Biswal et al., 1995; Beckmann et al., 2005; Raichle, 2015). These RSNs are constrained by, but not limited to, structural connectivity (Park and Friston, 2013) and resemble several networks of functionally connected regions modulated by active tasks such as the dorsal attention network (DAN), lateralized right and left fronto-parietal control networks (r-FP and l-FP, respectively), executive network, motor network, visual network, and default mode network (DMN). It has been suggested that spontaneous BOLD signal fluctuations have neurophysiological origins (Raichle, 2010; Shmuel and Leopold, 2008; Tagliazucchi et al., 2012). Previous studies attempted to correlate the power of specific EEG rhythms with resting-state measurements and showed that RSNs are related not only to one brain rhythm, but to combinations of several. In terms of the BOLD signal amplitude in resting-state networks, global (i.e., average over all EEG channels), as well as particularly occipital, alpha (8–13 Hz) power has been positively correlated with DMN and negatively correlated with DAN, r-FP, l-FP, and visual networks (Mantini et al., 2007; Mo et al., 2013; Zhan et al., 2014). Global beta (13–30 Hz) power has been positively correlated with DMN and negatively correlated with DAN, visual and motor networks (Mantini et al., 2007). Global gamma (>30 Hz) power has been positively correlated with global resting-state activity and, in particular, with regions from the executive network (e.g., medial-ventral prefrontal cortex and anterior cingulate (Mantini et al., 2007)). In terms of functional connectivity (expressed as temporal correlations), special attention has been paid to occipital alpha power, which negatively correlates with functional connectivity within visual cortices and between visual and more frontal and subcortical regions (Scheeringa et al., 2012). An inverse relationship has also been reported between central alpha and beta power spectra and changes in functional connectivity, mostly between subcortical regions and association cortices. In addition, a positive relationship has been found between gamma power and functional connectivity changes between subcortical, association and primary cortices (central and occipital gamma power) and within these regions (frontal gamma power) (Tagliazucchi et al., 2012). These links between specific EEG frequencies and RSNs motivate the possibility of probing RSNs by modulating oscillatory activity with tACS.

The aim of the present study was to evaluate whether tACS applied over occipital and parietal cortices induces changes in spontaneous activity measured with rs-fMRI. To this end, we applied tACS at three different frequencies in the alpha, beta, and gamma range (10, 16, 40 Hz, respectively), and with two different electrode montages (Cz-Oz and P5–P6). The tACS frequencies and electrode montages were chosen based on previous studies showing modulatory effects of tACS at alpha or gamma frequencies on visual perception (Helfrich et al., 2014a; Laczo et al., 2012; Wang et al., 2015; Cabral-Calderin et al., 2016).

Given that our previous fMRI study indicated strongest tACS effects in regions that were distant from the electrodes (i.e., fronto-parietal but not occipital regions) (Cabral-Calderin et al., 2016), (I) we hypothesized that tACS would change functional connectivity between directly stimulated regions and more distant areas. Based on previous EEG/fMRI and tACS/fMRI studies, (II) we expected to observe frequency-dependent modulation of RSNs with tACS. Given the previously reported negative correlations between the power of alpha/beta rhythms and functional connectivity, as well as BOLD signal amplitude in most RSNs (Tagliazucchi et al., 2012; Mantini et al., 2007; Scheeringa et al., 2012), (III) we hypothesized that tACS at alpha and beta frequencies should reduce the amplitude of spontaneous low frequency fluctuations and functional connectivity in most RSNs (e.g., DAN and visual network). An exception should be observed in the DMN, where the power of alpha and beta rhythms have been found to positively correlate with that network's BOLD signal amplitude, therefore, (IV) alpha and beta tACS should increase the amplitude of spontaneous low frequency fluctuations in the DMN (Mantini et al., 2007; Mo et al., 2013). Since gamma power has been positively associated with the amplitude of BOLD signal fluctuations and their correlations (Tagliazucchi et al., 2012; Mantini et al., 2007), (V) tACS in the gamma range should increase the amplitude of spontaneous low frequency fluctuations and functional connectivity. According to our previous study (Cabral-Calderin et al., 2016) we hypothesized that (VI) the strongest modulation of spontaneous low frequency fluctuations would be observed with alpha/beta tACS mainly in fronto-parietal networks (i.e., r-FP and l-FP). In addition, since different electrode positions induce different electric field distributions (Neuling et al., 2012; Windhoff et al., 2013), (VII) we expected to observe a difference in the low frequency fluctuation changes associated with each electrode montage. Based on a previous study that simulated the electric field distribution induced by transcranial electric stimulation (Neuling et al., 2012), (VIII) we expect tACS over Cz-Oz to stimulate mainly occipital cortex and, as a result, to modulate the amplitude of low frequency fluctuations and functional connectivity relative to the visual network. Following the same reasoning, (IX) tACS over P5–P6 should stimulate mainly parietal regions, translating into modulation of the amplitude of low frequency fluctuations in parietal cortices and functional connectivity of RSNs involving parietal regions such as r-FP, l-FP and DAN.

Methods

Transcranial alternating current stimulation (tACS)

A battery-driven Eldith DC-stimulator Plus (NeuroConn GmbH, Ilmenau, Germany) delivered tACS through a pair of conductive rubber electrodes attached with electrode paste (Weaver and Company,

Aurora, CO). Two different electrode montages were used in the experiment: (1) electrodes placed over Cz-Oz, (2) electrodes placed over P5–P6, as determined by the International 10–20 EEG system (Fig. 1A). Each montage was comprised of two round electrodes with each electrode covering an area of 16 cm^2. The stimulation sites were chosen to induce oscillations bilaterally in occipital and parietal cortices (Neuling et al., 2012; Windhoff et al., 2013). For both montages, tACS was applied at 10, 16, and 40 Hz for 8 min. The waveform of the stimulation was sinusoidal without DC offset. The current was fixed to 1 mA (peak-to-peak), resulting in a mean current density of 0.063 mA/cm^2 (peak-to-peak) under each electrode. The current was ramped up and down over 1 s in order to make the protocol more comparable to our previous study (Cabral-Calderin et al., 2016). Impedance was kept below 20 kΩ (impedances below 10 kΩ, as commonly used in tACS studies, cannot be accomplished because our MR-compatible stimulation setup has a minimum possible impedance of 11.8 kΩ (Cabral-Calderin et al., 2016)). Previous studies using similar tACS equipment have reported no significant artifacts induced by tACS on the BOLD signal (Cabral-Calderin et al., 2016; Antal et al., 2014). However, possible artifacts induced by electrical stimulation might be specific to imaging and stimulation parameters. In order to evaluate possible tACS-induced artifacts, we performed additional scanning sessions with a phantom, using the same tACS parameters that were used in the main experiment. In agreement with our previous study (Cabral-Calderin et al., 2016), we observed differences in the temporal signal-to-noise ratio (tSNR) when compared between scans with (i.e., electrodes placed and connected to the tACS stimulator outside the shielded room) or without tACS setup. However, tSNR values were stable when comparing tACS-on with tACS-off, while keeping all the other conditions the same. In our study, the tACS setup was always in place and, therefore, we do not expect tACS-induced artifacts to influence our results. Each subject participated in a total of six sessions, in each of which tACS was applied with a single tACS frequency-electrode montage combination in a randomized order. Each session was conducted on a different day, separated by at least 48 h (average time between experimental sessions across subjects: 208 h, SD: 117 h).

Magnetic resonance imaging (MRI)

Experimental setup and design

Twenty subjects (10 females, mean age 25.1 ± 3.1 years) with normal or corrected-to-normal vision and without history of neurological or psychiatric disease took part in the study. All subjects gave written informed consent. All procedures were performed according to the declaration of Helsinki and approved by the local Ethics Committee of the University Medical Center Göttingen. All subjects were naive to the purpose of the experiments and were paid for their participation.

In each of the six sessions, a total of six resting-state scans were collected. Each resting-state scan lasted ~8 min, during which subjects were asked to remain still with eyes open while fixating on a central cross. Eye position was monitored using an MR-compatible eye tracking system (Arrington Research, Inc., Scottsdale, AZ) to verify that subjects remained awake and fixating on the central cross throughout the resting-state scan. The first three resting-state scans of each session referred to pre-sham, sham, and post-sham conditions. During the sham condition, tACS was applied with the same parameters as the active stimulation but with a total duration of 10 s. In each session, the last three resting-state scans referred to pre-stimulation, stimulation, and post-stimulation conditions. During the stimulation condition, tACS was applied with a total duration of 8 min. The sham and active stimulation blocks were separated by at least 8 min (in which anatomical data were collected). In each session, the sham stimulation block preceded the active stimulation block to prevent after-effects of long stimulation from contaminating sham conditions. After each run, the subjects rated the strength of perceived phosphenes, cutaneous sensation, and fatigue intensities on a scale ranging from 1 to 10. Due to technical problems in the first functional run of each session (lower tSNR with respect to the other runs within the session), this run (pre-sham) was not used for analysis. Therefore, the sham condition for each of the different frequencies was not included in the final analyses. The post-sham run was used for defining RSNs (see Methods) and, for simplicity, will be referred to as "baseline" throughout the manuscript. The session flow is depicted in Fig. 1B.

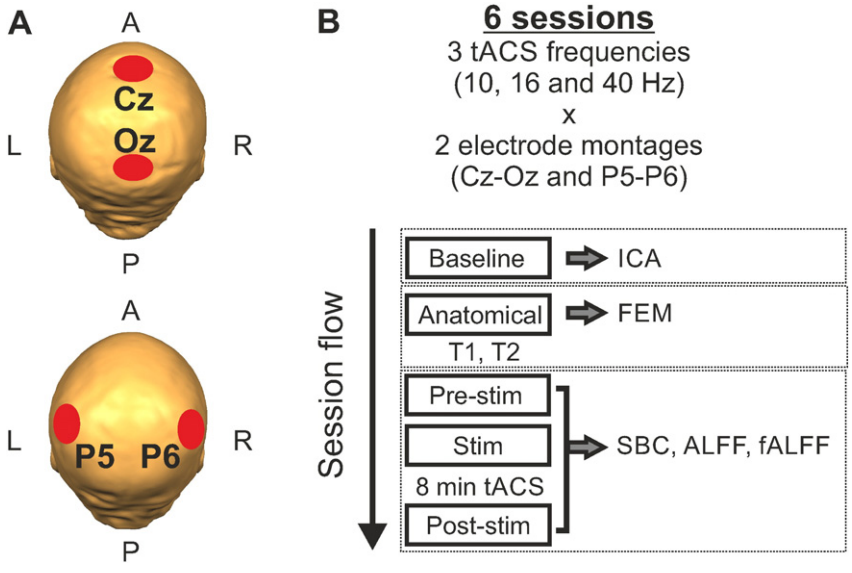

Fig. 1. Experimental design. A) The two electrode montages used in our experiment are illustrated with colored circles on top of a 3D reconstruction of one example participant. L: left, R: right, A: anterior, P: posterior. B) Session flow. Each session included a baseline and three stimulation runs (pre-stimulation, stimulation and post-stimulation) separated by one anatomical measurement (T1-weighted/T2-weighted with/without fat saturation). The session flow was kept constant across sessions but the tACS condition (frequency x electrode montage combination) and the type of anatomical measurement collected in each session were pseudorandomized across participants. Dashed boxes on the right of the panel contain depictions of the analysis implemented with the dataset collected in the specific run. ICA: independent component analysis for defining the resting-state networks, FEM: finite element method simulations, SBC: seed-based functional connectivity analysis, and ALFF: amplitude of low frequency fluctuations and its fraction (fALFF).

Data acquisition

All images were acquired using a 3 Tesla Magnetom TIM Trio scanner (Siemens Healthcare, Erlangen, Germany) with a 32-channel phased-array head coil. First, a high-resolution T1-weighted anatomical scan (three-dimensional (3D) turbo fast low angle shot; repetition time (TR): 2250 ms, inversion time (TI): 900 ms, echo time (TE): 3.26 ms, flip angle 9°, isotropic resolution of $1 \times 1 \times 1$ mm^3) was obtained. All functional data were acquired using the 2D multiband gradient-echo echo-planar imaging sequence from the Center for Magnetic Resonance Research, University of Minnesota (Xu et al., 2013; Moeller et al., 2010; Setsompop et al., 2012) with T2*-weighting (TR: 900 ms, TE: 30 ms, flip angle 50°, 39 slices of 3-mm thickness, gap between slices of 10%, in-plane resolution of 3×3 mm^2, multiband acceleration factor 3). A total of 544 whole-brain volumes were acquired in each functional run. In the stimulation run, tACS was initiated after 10 volumes were acquired. Six additional anatomical datasets were collected, one in each session, between sham and active stimulation blocks. Four of these datasets were used for creating individualized finite element method (FEM) head models for the electric field simulations (see section below, (Windhoff et al., 2013; Thielscher et al., 2015)). These four anatomical datasets consisted of two T1-weighted anatomical scans with the parameters described above, with and without fat suppression, and two T2-weighted anatomical scans (3D turbo spin echo; TR: 3500 ms, TE: 282 ms, variable flip angle, with integrated parallel acquisition technique: factor 2, isotropic resolution of $1 \times 1 \times 1$ mm^3), with and without fat suppression. The other two anatomical datasets were not used for any further analyses but were collected in order to have the same time interval between the sham and active stimulation blocks in all the six sessions.

Electric field simulations

The FEM models simulating the electric field induced by tACS were calculated using SimNibs (Windhoff et al., 2013; Thielscher et al., 2015). One participant was excluded from the electric field simulations due to a mesh generation error with one of the anatomical datasets. For the remaining 19 subjects, each subject's set of T1- and T2-weighted images (with and without fat suppression) was used to create an individualized FEM mesh for modeling the electric field for the electrode montages used in this experiment. Inconsistencies in head meshes due to electrode deformations were corrected manually. Electrode position coordinates were determined using a virtual 10–20 cap placed on the mesh based on each subject's anatomy using customized Matlab scripts (Matlab R2011b, www.mathworks.com, Natick, MA). Electric field simulations were generated in SimNibs for Cz-Oz and P5–P6 electrode placements for each subject using standard tissue conductivities of $\sigma_{skin} = 0.465$ S/m, $\sigma_{skull} = 0.010$ S/m, $\sigma_{CSF} = 1.654$ S/m, $\sigma_{GM} = 0.275$ S/m, $\sigma_{WM} = 0.126$ S/m, for skin, skull, cerebral spinal fluid (CSF), gray matter and white matter (WM), respectively (Thielscher et al., 2011). To generate regions of interest (ROI) for seed-based functional connectivity analysis, the electric field strength (norm E) for each simulation was transformed to corresponding subject gray matter masks segmented from original MR volume space. The resulting MR-space electric field simulation data were Talairach transformed, thresholded at 50% of the maximum electric field of each map (Opitz et al., 2015a), and binarized. Binarized electric field masks were overlaid for all subjects for a given electrode montage and then thresholded such that any voxel in which four or more subjects had 50% or greater electric field strength for the given montage was included. The resulting thresholded group mask was used as a seed for cross-correlation analysis for each electrode position, except Cz, which left only a few voxels, as is evident from the group participation maps (Supplemental materials, Fig. S1). Seeds for P5 and P6 electrode positions were separated using a right-left hemisphere mask in Talairach space. For each subject, the mean electric field strength from the 50% thresholded map was extracted for each electrode montage and used to quantitatively characterize the single subject's electric field properties. The extracted values were used for comparing the electric field strength induced by each electrode montage at the group level using *paired t-test* as implemented in STATISTICA version 12.

Functional MRI data analysis

Preprocessing

All data preprocessing was performed in AFNI (Cox, 1996). The first 10 volumes were discarded to align stimulation start time to the functional data. Preprocessing steps included: despiking, slice timing correction, deobliquing, motion correction, resampling to $3 \times 3 \times 3$ mm, transformation to Talairach space using each session's T1-to-MNI152 standard template transformation (MNI template was transformed to Talairach space using AFNI's 3dWarp in order to ensure compatibility between software used for individual processing and group statistical analyses), and 6 mm full-width-at-half-maximum-kernel Gaussian smoothing. With the exception of data used for creating the RSN seeds, the following preprocessing steps were also implemented: 4th-order polynomial regression (equivalent to demeaning, linear trend removal, and high-pass filtering), regression of motion parameters and the first derivative of the motion parameters, bandpass filtering between 0.01 and 0.1 Hz, and nuisance regression of WM and CSF signals extracted from masks segmented from individual anatomical data.

Amplitude of low frequency fluctuations (ALFF) and fractional ALFF (fALFF) analysis

The ALFF and fALFF were computed for all runs using AFNI (Zang et al., 2007; Zou et al., 2008). Both ALFF and fALFF measure the power of low frequency fluctuations, which gives an indication of local metabolic changes associated with the BOLD signal. The algorithm was run on the preprocessed data before bandpass filtering. Briefly, on a voxel-by-voxel basis, the time course was converted into the frequency domain using a Fast Fourier Transform, the square root of the power spectrum was computed, and the average of the amplitudes in the range of 0.01–0.1 Hz were then calculated to obtain the ALFF (Zang et al., 2007; Zou et al., 2008). Dividing each voxel's ALFF value by the amplitudes of the entire detectable frequency range (0–0.55 Hz) yields that voxel's fALFF (Zou et al., 2008) (Supplemental materials, Fig. S2A). Both ALFF maps and fALFF maps were standardized with Z transformation (subtract global mean and divide by standard deviation) prior to statistical analyses. While the ALFF reports the absolute power of low frequency fluctuations, it can be sensitive to high frequency pulsatile changes such as heart rate, an artifact that can be mitigated by considering the fALFF, which has reduced sensitivity to such noise sources but lower test-retest reliability (Zuo et al., 2010). Thus, it is important to consider both measures. In our dataset, ALFF results closely resembled fALFF results and therefore are not shown or described.

Seed-based functional connectivity analysis

Cross-correlation analyses were carried out in AFNI. Two different sets of ROI seeds were defined for these analyses. The first set was defined to represent commonly used RSNs using independent component analysis (ICA), and the second set consisted of seeds derived from the electric field simulation, as described in the previous section ('*Electric field simulations*').

In order to define group-level, subject-based RSNs for analysis of effects of tACS on intrinsic functional connectivity, temporal concatenation group ICA was performed on the baseline run from every session of every subject using FSL's MELODIC toolbox (Jenkinson et al., 2012). Using the baseline run from every imaging session allows for group-level definition of independent components without the use of the experimental data (pre-stimulation, stimulation, and post-stimulation runs), which is subsequently used for evaluating tACS-effects. In addition, including runs from all sessions can account for day-to-day subject

variability in the RSNs. The algorithm was run on preprocessed data before any nuisance regression or bandpass filtering and was fixed to extract 30 components. Choosing 30 independent components allowed reliable extraction of the seven RSNs that we chose to focus on; that is, the DAN, DMN, executive, visual, motor, l-FP, and r-FP networks. We chose these networks because we were interested in tACS effects in well-known RSNs (Fox et al., 2005; Beckmann et al., 2005). The resulting group components were then used to create ROI masks for seed-based functional connectivity analysis by binarizing 50% of the maximum positive signal from each of the chosen components. The ICA components chosen for the purpose of our analysis, as well as the corresponding seeds derived for calculating functional connectivity, are depicted in Fig. 2. A graphical representation of the procedure can be found in Supplemental materials Fig. S2 B. Since the 50% mask of the DAN seed did not include the bilateral parietal regions (Fox et al., 2005), we chose the mask threshold (70%) that included left and right intraparietal sulci.

Network-to-network functional connectivity. As a strategy of data reduction, a network-to-network functional connectivity approach was conducted in order to evaluate first the gross impact of tACS on intrinsic functional connectivity between RSNs. For each condition of an individual subject, the average time course extracted for each RSN was correlated with that of every other network using Pearson's correlation. The correlation values were transformed with the Fisher's r-to-z procedure in order to be able to conduct statistical analyses on correlation values. The resulting z-transformed correlations are summarized in a 7×7 inter-network functional connectivity matrix in Supplemental materials (Fig. S2 B).

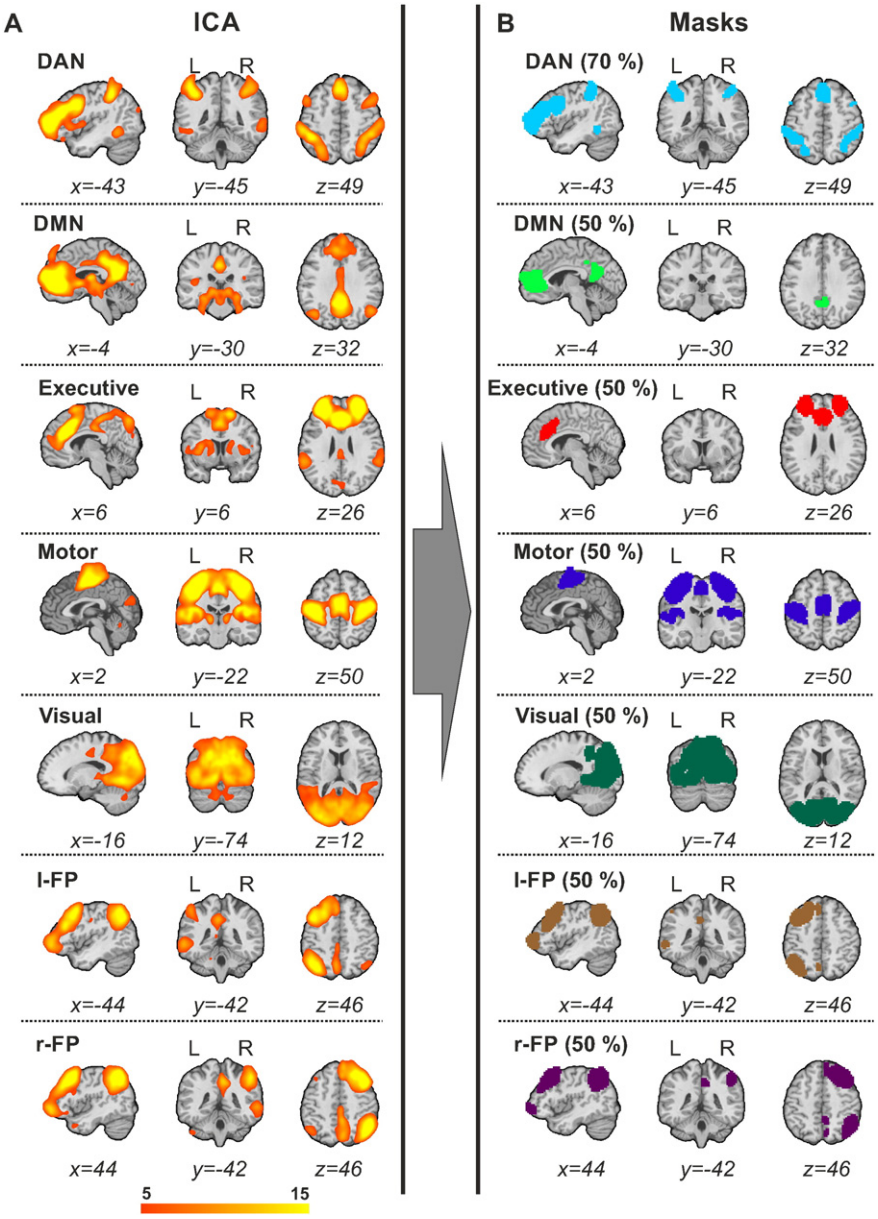

Fig. 2. ICA results. A) Selected components representing the seven resting-state networks selected for further analysis (from top: dorsal attention network (DAN), default mode network (DMN), executive network, motor network, visual network, left fronto-parietal control network (l-FP) and right fronto-parietal control network (r-FP). B) Masks created from each component (thresholded at 50% or 70%) representing each network to be used in the SBC.

Whole-brain functional connectivity. For each stimulation run (pre-stimulation, stimulation, and post-stimulation) of each subject, whole-brain functional connectivity was computed for all aforementioned seeds. Each seed was resampled into functional data resolution ($3 \times 3 \times 3$ mm^3) and used as a mask to extract the average time course from the ROI. For a given seed, the resulting time course was then correlated with that of every other voxel in the brain using Pearson's correlation. The resulting coefficient indexes how temporally similar any voxel in the brain is to the network or region in question; thus, as measured with BOLD contrast, seed-based functional connectivity is always an indication of the functional state of the brain relative to the seed of interest. Supplemental materials (Fig. S2 B, C) illustrate the general scheme for obtaining whole-brain correlations on the basis of RSN and electric field simulation-based seeds, respectively. Finally, for a total of ten seeds (7 RSNs, 3 electric field simulation-based ROIs), six sessions and three (pre-stimulation, stimulation, post-stimulation) runs, 180 whole-brain correlation maps were computed for each subject. Correlation maps were Fisher r-to-z transformed prior to statistical analyses.

Statistical analysis

All statistical comparisons were performed between the different tACS frequencies and electrode montages for the active stimulation (pre-stimulation, stimulation, and post-stimulation), combinations of which were applied in a pseudorandomized manner across subjects and sessions. This way, each frequency and electrode montage combination works as an implicit control condition for the others, controlling for placebo effects, which should be universal across conditions. For this reason, we focus on tACS frequency- and electrode montage-dependent effects but not on non-specific tACS effects.

Network-to-network functional connectivity

Statistical analyses were implemented in STATISTICA. To obtain a general overview for evaluating the impact of tACS on the functional connectivity between networks, we analyzed the 7×7 inter-network functional connectivity matrices. A four-factor repeated measures analysis of variance (rANOVA) was conducted for each network with the within factors tACS frequency (3 levels: 10, 16, and 40 Hz), electrode montage (2 levels: Cz-Oz and P5–P6), time (3 levels: pre-stimulation, stimulation, and post-stimulation) and network combination (6 levels: e.g., for DAN the network combinations were DAN-DMN, DAN-executive, DAN-motor, DAN-visual, DAN-l-FP, and DAN-r-FP). Accordingly, seven different four-factor rANOVAs were conducted. In cases that the rANOVA showed significant interaction effects (e.g., interaction tACS frequency $\times$ electrode montage $\times$ time $\times$ network), a three-factor rANOVA was conducted for each level of the network combination factor while keeping the remaining factors as in the original four-factor rANOVA. In cases of significant interactions, post-hoc analyses were performed using *paired t-tests* to further explore the differences.

Whole-brain functional connectivity and fALFF

All group-level volume statistics were conducted using BrainVoyager QX Software version 2.8 (Brain Innovation, Maastricht, The Netherlands), and the Neuroelf 0.9c toolbox for Matlab (retrieved from http://neuroelf.net/). For fALFF and network-to-whole-brain functional connectivity, statistical analyses were done using a three-factor rANOVA with the within factors tACS frequency (3 levels: 10, 16, and 40 Hz), electrode montage (2 levels: Cz-Oz and P5–P6), and time (3 levels: pre-stimulation, stimulation, and post-stimulation). For correlation maps resulting from P5, P6, and Oz seeds, two-factor rANOVAs were applied using only conditions where tACS was applied with the respective electrode montage. For Oz seed-based maps, a two-factor rANOVA with the within factors tACS frequency (3 levels: 10, 16, and 40 Hz) and time (3 levels: pre-stimulation, stimulation, and post-stimulation) was conducted for Cz-Oz stimulation conditions. For P5 and P6 seed-based maps, similar two-factor rANOVAs were conducted for P5–P6 stimulation conditions. For all whole-brain analyses, in cases of statistical significance in the rANOVAs, the standardized fALFF or Fisher's z-transformed correlation values were extracted from each significant cluster and post-hoc analyses were conducted using *paired t-tests* as implemented in STATISTICA.

For all statistical maps, multiple comparisons correction was performed at the cluster level. Maps were thresholded at an initial cluster-forming threshold of $p < 0.005$. The sizes of the resulting clusters were assessed for significance using Monte Carlo simulations as implemented in BrainVoyager's cluster-level statistical threshold estimator plugin. Reported clusters are significant at a level of $p < 0.05$. For labeling the significant regions, the peak activation voxel from each cluster was entered into the Talairach client tool (Research Imaging Institute, http://www.talairach.org/client.html), a 5 mm range cube was defined around the peak voxel and the cluster was labeled according to the region to which most of the defined voxels belong. The statistical volume maps in the figures are overlaid on the Colin brain template.

Phosphene perception, cutaneous sensation and fatigue ratings

Statistical analyses for phosphene perception, cutaneous sensation, and fatigue ratings were performed using a three-factor rANOVA with the within factors tACS frequency (3 levels: 10, 16, and 40 Hz), electrode montage (2 levels: Cz-Oz and P5–P6) and time (3 levels: pre-stimulation, stimulation, and post-stimulation). In cases of statistical significance, post-hoc analyses were conducted by using *paired t-tests* as implemented in STATISTICA. Additional analyses were performed correlating phosphene perception and cutaneous sensation ratings with the fALFF values extracted from ROIs located in the corresponding primary sensory cortices. The detailed procedure is described in Supplemental materials.

Results

Electric field simulations

Using a finite element method, the electric field for each montage was simulated for every participant in order to predict the regions being directly stimulated by tACS. According to the simulation, the electric field induced by tACS over Cz-Oz is more centered on the occipital cortex while the electric field induced by tACS over P5–P6 is more centered over parietal areas in both hemispheres, as can be viewed in a representative subject shown in Fig. 3. Although the region of maximum stimulation is different for each electrode montage, some areas receiving lower electric fields are shared in both montage setups, primarily in medial occipito-parietal areas. Visual inspection of the electric field simulations showed that the electric field is stronger and more widespread for tACS over P5–P6 than for tACS over Cz-Oz. This might be due to the proximity of the electrodes to the brain and CSF in each montage as well as the composition of the skull in the regions directly underneath the electrodes (Opitz et al., 2015b). For instance, CSF is one of the most conductive materials in the head, and therefore, it constitutes a less resistive path for the applied electric currents (Opitz et al., 2015b). With Cz-Oz, the electrodes are directly above a larger volume of CSF than P5–P6 electrodes, thus possibly shunting the highest electric field to regions of the brain not directly underneath the electrodes. On the contrary, with the P5–P6 montage, generally only a thin layer of CSF sits between the skull and the brain, thus possibly less current is carried away before entering the gray matter regions underneath the electrodes. In fact, it has been previously reported that gray matter regions that have a thin overlying CSF layer exhibit higher electric fields than those overlaid with a thick CSF layer (Opitz et al., 2015b). In addition, individuals' electric fields are the strongest in subjects with the thinnest layer of CSF (Laakso et al., 2015). The group participation maps for each electrode montage, in which the single-subject electric field maps transformed to MRI space and thresholded at 50% are overlaid

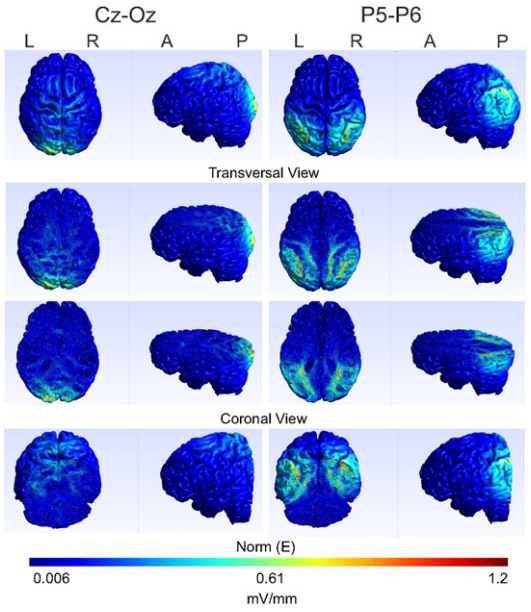

Fig. 3. Electric field distributions obtained from the finite element method simulations for each electrode montage for a representative subject. L: left hemisphere, R: right hemisphere, A: anterior, and P: posterior.

on a representative brain, are shown in Fig. S1. As expected from visual inspection of the maps, a *paired t-test* analysis on the mean electric field strength extracted from each subject's 50% thresholded map showed that the mean electric field induced by P5–P6 was stronger than that induced by Cz-Oz ($t(18) = 5.05, p < 0.001$). Overall, the mean strength of the electric field maps (within the 50% thresholded maps) did not show high variability across subjects. Nonetheless, inter-subject variability was higher for Cz-Oz than for P5–P6 (Cz-Oz: *mean* = 0.40 mV/mm, *SD* = 0.09, *range* = 0.31; P5–P6: *mean* = 0.51 mV/mm, *SD* = 0.08, *range* = 0.27).

Taken together, individual electric field simulations as well as the group participation maps suggest that direct effect of tACS with our electrode montages is expected over occipital (Cz-Oz) and parietal (P5–P6) areas.

Effect of tACS on fALFF

We investigated tACS-induced changes in the fALFF, which represents the intensity of spontaneous regional brain activity (Methods, Supplemental materials, Fig. S2A). With this approach, we evaluated local changes in resting-state activity independent of functional connectivity measures, which require interpretations relative to particular regions of interest (Zang et al., 2007; Zou et al., 2008). The three-factor rANOVA, evaluating the main effect of tACS frequency, electrode montage, time, and their interactions, showed a significant main effect of time ($F(2, 38) > 6.11, p < 0.005$) mainly in frontal and occipital regions, which in most cases was observed as a decrease in fALFF over time. However, since the order of the different levels (pre-stimulation, stimulation and post-stimulation) in the time factor is fixed, the effect of time cannot exclusively be attributed to tACS effects. Time effects could also manifest through cognitive state or scanner-related factors that systematically fluctuate over time (Chang and Glover, 2010; Murphy et al., 2013). Therefore, for this and the remainder of the statistical analyses, we do not report main effects of time, but focus our attention on the interactions: tACS frequency × time, electrode montage × time, and tACS frequency × electrode montage × time. With this approach, we control for time and placebo effects, which should be universal across conditions. These interactions could be understood as follows: the tACS frequency × time interaction shows the effect of time that is dependent on the tACS frequency (frequency-dependent effects), regardless of the electrode montage (the effect of frequency can be similar across electrode montages); the electrode montage × time interaction shows the effect of time that is dependent on the electrode montage (montage-dependent effects), regardless of the frequency (the effect of electrode montage can be similar across frequencies); and the tACS frequency × electrode montage × time interaction shows significant interaction between the frequency- and montage-dependent effects (frequency-dependent effects are different between electrode montages). Significant tACS frequency × time interaction ($F(4, 76) > 4.05, p < 0.005$) was found in a few clusters, including the precuneus (PCu) and the right middle occipital gyrus (MOG) (Fig. 4A). Post-hoc analyses on these clusters showed that, in general, tACS effects on fALFF were almost exclusively found in the post-stimulation period with opposite effects induced by 10 and 40 Hz tACS. In some regions, the effect of tACS at 16 Hz followed the effect of 10 Hz tACS (PCu) and in other regions, it followed that of 40 Hz tACS (MOG). Significant electrode montage × time interaction ($F(2, 38) > 6.11, p < 0.005$) was observed in a few clusters, including the cuneus (Cu) and the right medial frontal gyrus (MedialFG) (Fig. 4B). Post-hoc analyses on these clusters showed opposite effects induced by each electrode montage during and after the stimulation period. In general, the observed trend was that, in the most posterior regions (e.g., Cu), tACS over Cz-Oz increased the fALFF during the stimulation, which decreased or returned to pre-stimulation levels in the post-stimulation period, while tACS over P5–P6 decreased fALFF mainly in the stimulation period. The tACS frequency × electrode montage × time interaction was significant ($F(4,76) > 4.05, p < 0.005$) for a few clusters, including bilateral postcentral gyrus (PoC) close to primary motor/somatosensory cortices, and the inferior parietal lobule (IPL) (Fig. 4C). Post-hoc analyses showed that for PoC, tACS at 10 Hz increased fALFF during the stimulation period when it was applied over Cz-Oz while it decreased fALFF during and after the stimulation when it was applied over P5–P6. A different pattern was observed for IPL, where 10 Hz decreased fALFF when it was applied over Cz-Oz and it increased fALFF when applied over P5–P6, both effects observed during the stimulation but not after. The effects of 16 and 40 Hz tACS were observed in PoC where 16 Hz P5–P6 and 40 Hz Cz-Oz decreased fALFF, both effects observed only in post-stimulation. A detailed description of the three-factor rANOVA results – including statistical values for each cluster that showed a significant interaction effect as well as the post-hoc test performed on the fALFF values extracted from the specific cluster – is provided in Supplemental materials, Table 1.

In a complementary analysis, it was observed that for some tACS conditions, the mean strength of the electric field induced by tACS predicted the stimulation effects mainly in posterior regions. For instance, subjects exhibiting higher mean electric field strengths with the Cz-Oz montage showed higher decreases in fALFF values in posterior regions, such as PCu and the left fusiform gyrus (both during stimulation), due to 10 Hz tACS over Cz-Oz ($r < -0.62, p < 0.005$). A detailed description of these results is provided in Supplemental materials (Results, Fig. S3, Table 2).

Taken together, fALFF analysis indicates that tACS affected the regional metabolic activity in a frequency- and electrode montage-dependent manner during and after the stimulation period, with 10 and 40 Hz tACS inducing opposite effects. Electrode montage-dependent effects were observed in a few regions close to the electrodes (i.e., PoC and IPL), but specific regional effects were not exclusive to their correspondingly expected montage. For example, based on simulations, we would expect IPL modulation only with tACS over P5–P6, however, both montages showed significant effects, albeit in opposite directions. The significant correlations observed between the electric field strength and the effect of tACS on fALFF suggests that incorporating individual predictions based on electric field simulations could be a valuable approach for evaluating tACS effects in both, neural and behavioral studies.

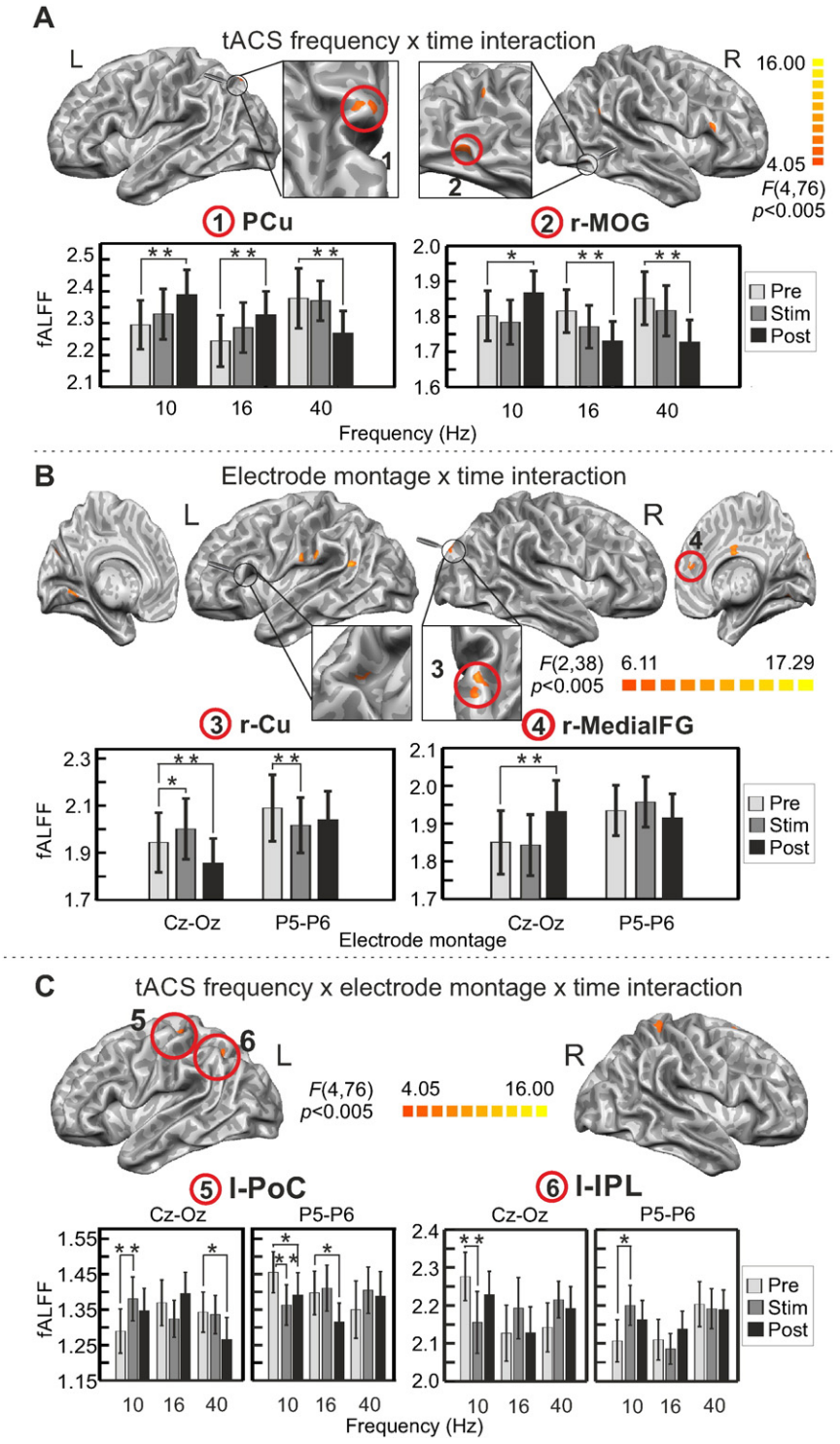

Fig. 4. Effect of tACS on fALFF. Significant interactions in the three-factor rANOVA performed on the fALFF overlaid on the surface-rendered Colin brain template. A) tACS frequency × time interaction, B) Electrode montage × time interaction, and C) tACS frequency × electrode montage × time interaction. Maps were thresholded using clusters determined by $p < 0.005$ and a corrected cluster significance threshold of $p < 0.05$. The resulting cluster size threshold was 6 functional voxels (162 mm) for A and 7 functional voxels (189 mm) for B and C. Bar graphs show post-hoc results for representative clusters for each interaction effect. Error bars denote standard error of the mean. L: left hemisphere, R: right hemisphere. MOG: middle occipital gyrus, PCu: precuneus, Cu: cuneus, MedialFG: medial frontal gyrus, PoC: postcentral gyrus, and IPL: inferior parietal lobe. $^{*}p < 0.05$, $^{**}p < 0.01$.

Effect of tACS on resting-state network functional connectivity (seed-based functional connectivity analysis)

Network-to-network functional connectivity changes

After evaluating tACS-induced changes in fALFF as a measure of intensity of spontaneous regional brain activity, we next focused on evaluating tACS-induced changes on functional connectivity expressed by temporal correlations. Seven well-known resting-state networks (Fox et al., 2005; Beckmann et al., 2005) were defined from the baseline scans using temporal concatenation group ICA (Methods, Fig. 2A). The main components resulting from the ICA matched the previously reported RSNs (Fox et al., 2005; Biswal et al., 1995; Beckmann et al.,

2005; Corbetta and Shulman, 2002; Gao and Lin, 2012; Raichle et al., 2001; Amadi et al., 2013; Lowe et al., 1998; Spreng et al., 2013; Vincent et al., 2008). The selected component representing the DAN included regions located bilaterally along the intraparietal sulci (IPS), frontal eye fields (FEF), human visual motion complex (V5/hMT+), and part of the MedialFG (Fox et al., 2005; Corbetta and Shulman, 2002; Gao and Lin, 2012). The DMN component included bilateral angular gyri and, most strongly, anterior and posterior cingulate cortices (ACC/PCC) (Fox et al., 2005; Gao and Lin, 2012; Raichle et al., 2001). The executive network component included cingulate gyrus (CG) and bilateral middle frontal gyrus (MFG)/superior frontal gyri (SFG) (Beckmann et al., 2005; Amadi et al., 2013). The motor network component included bilateral pre-central gyrus (PrC) and PoC, insula and supplementary motor area (SMA) (Biswal et al., 1995). The visual network component included mainly occipital cortex (Lowe et al., 1998). The components representing the r-FP and l-FP included regions in the MFG, inferior temporal gyrus (ITG), PCu and IPL/superior parietal lobe (SPL), located in the right and left hemispheres, respectively (Gao and Lin, 2012; Spreng et al., 2013; Vincent et al., 2008). These components were thresholded at 50% (except for DAN, which was thresholded at 70%) and used to represent RSNs (Fig. 2B) in seed-based functional connectivity analysis.

To obtain a general overview of the impact of tACS on resting-state functional connectivity, we first evaluated between-network correlation changes. To this end, seed-based functional connectivity analysis was conducted by correlating each RSN's average time course with that of every other network (Methods, Supplemental materials, Fig. S2 B). Visual inspection of the network-to-network results (Supplemental materials, Fig. S4) shows that the functional connectivity pattern between networks remained similar in all conditions (i.e., tACS frequency, electrode montage, and time). As reported in the literature of resting-state functional connectivity, there was an anticorrelation between DAN and DMN, and positive correlations between DAN and the fronto-parietal control networks (l-FP and r-LP) (Fox et al., 2005; Gao and Lin, 2012). The four-factor rANOVA evaluating the main effects and interactions between tACS frequency, electrode montage, time, and network combination was significant only for the DAN (tACS frequency × electrode montage × time × network interaction: $F\ (20, 380) = 1.66$, $p = 0.037$) and for the l-FP (tACS frequency × time × network interaction: $F\ (20, 380) = 1.71$, $p = 0.029$; tACS frequency × electrode montage × time × network interaction: $F\ (20, 380) = 1.97$, $p = 0.007$). Follow-up three-factor rANOVAs for the functional connectivity between each of these networks (DAN and l-FP) and the remaining six RSNs showed significant tACS frequency × electrode montage × time interaction for the DAN to visual network combination ($F\ (4, 76) = 2.70$, $p = 0.036$). With respect to the l-FP, a significant tACS frequency × time interaction was observed for the combination l-FP to visual network ($F\ (4, 76) = 3.16$, $p = 0.018$), and a significant tACS frequency × electrode montage × time interaction was observed for the functional connectivity of l-FP to DMN ($F\ (4, 76) = 2.64$, $p = 0.040$). It is worth noting that for the two above-mentioned significant tACS frequency × electrode montage × time interactions (DAN to visual network, l-FP to DMN), post-hoc analyses showed that tACS was effective only when applied over Cz-Oz, but not when applied over P5–P6. A more detailed description about the main effects and post-hoc analyses are shown in Supplemental materials, Fig. S5. In summary, tACS-induced modulation of the network-to-network functional connectivity was only significant for the DAN (i.e., with the visual network) and the l-FP (i.e., with the visual network and DMN), mainly with tACS over Cz-Oz.

Network-to-whole-brain functional connectivity changes

To gain further insight into network-based interactions, each RSN's average time course was correlated with that of every other voxel in the brain (Supplemental materials, Fig. S2 B). This approach offers the opportunity to evaluate functional connectivity changes within a network as well as between the network and the whole brain in a less categorical manner than the network-to-network analysis (Methods). We focus our description of the results on the networks that showed tACS-induced modulation in either the fALFF or the network-to-network analysis, i.e., DAN, l-FP, motor, and visual networks. Focus on the visual and l-FP networks was also motivated by the electric field simulation prediction that tACS at Cz-Oz and P5–P6 maximally stimulate occipital and parietal cortices, respectively. The DMN, executive network and the r-FP did not show significant tACS modulation in either fALFF or network-to-network analysis; therefore, we will not describe network-to-whole-brain analysis results for these networks.

Dorsal attention network (DAN). For the DAN (Fig. 5A), the functional connectivity maps obtained in the pre-stimulation conditions (Fig. 5B) are similar to the original DAN component obtained from the ICA (compare Fig. 5B to Fig. 2A). A significant tACS frequency × time interaction ($F\ (4, 76) > 4.05$, $p < 0.005$, Fig. 5C) was observed in a few clusters, including the right MOG and the left lentiform nucleus (LN), an anatomical region that comprises the putamen and the globus pallidus in the basal ganglia. In the case of the MOG, post-hoc analyses showed that its functional connectivity with the DAN was significantly modulated by tACS at 10 and 16 Hz, with 10 Hz decreasing functional connectivity and 16 Hz tACS increasing it. These changes were restricted to the stimulation period. For the LN, 10 and 16 Hz tACS increased functional connectivity during (10 Hz) or after (16 Hz) the stimulation period while 40 Hz decreased it both during and after the stimulation. Significant electrode montage × time interaction ($F\ (2, 38) > 6.11$, $p < 0.005$, Fig. 5D) was observed in the right MFG and most strongly in the bilateral thalamus. Post-hoc analyses showed that in both regions, tACS over Cz-Oz decreased its functional connectivity with the DAN while tACS over P5–P6 increased it, however, for the right MFG, these effects were observed only in the post-stimulation period, while for the thalamus, these effects were observed both during and after the stimulation period. A significant tACS frequency × electrode montage × time interaction ($F\ (4, 76) > 4.05$, $p < 0.005$, Fig. 5E) was observed mainly for the right superior temporal gyrus (STG) and for left IPL. Post-hoc analyses showed that for the right STG, 16 Hz tACS increased its functional connectivity with the DAN during the stimulation period when applied over Cz-Oz while 40 Hz decreased it in the post-stimulation period. For this cluster, 40 Hz tACS was the only effective frequency when tACS was applied over P5–P6, which increased the functional connectivity in the post-stimulation period. For the left IPL, 10 Hz tACS applied over Cz-Oz decreased its functional connectivity with the DAN during and after the stimulation period while it increased it in the post-stimulation period when applied over P5–P6. Stimulations with 16 and 40 Hz tACS were effective when applied over P5–P6, decreasing the left IPL-to-DAN functional connectivity during (16 and 40 Hz) and after (only 16 Hz) the stimulation period. A detailed description of the three-factor rANOVA results – including statistical values for each cluster that showed a significant interaction effect as well as the post-hoc test performed on the z-transformed correlation values extracted from the specific cluster – is provided in Supplemental materials, Table 3.

In general, tACS-induced modulation of the functional connectivity between the DAN and the whole brain was mainly observed in regions outside the network (e.g., right MOG). Within network changes were observed, for example, in the left IPL.

Left fronto-parietal control network (l-FP). For the l-FP (Fig. 6A), the correlation maps in the pre-stimulation conditions (Fig. 6B) resemble closely the original l-FP component obtained from ICA (compare Fig. 6B to Fig. 2A). The tACS frequency × time interaction was significant ($F\ (4, 76) > 4.05$, $p < 0.005$, Fig. 6C) in several regions in frontal, parietal and occipital cortices as well as in the LN. The largest clusters included one covering a broad area in the right occipito-parietal cortices and another in the LN. Post-hoc analyses showed that 10 Hz tACS increased functional connectivity between l-FP and these two clusters while

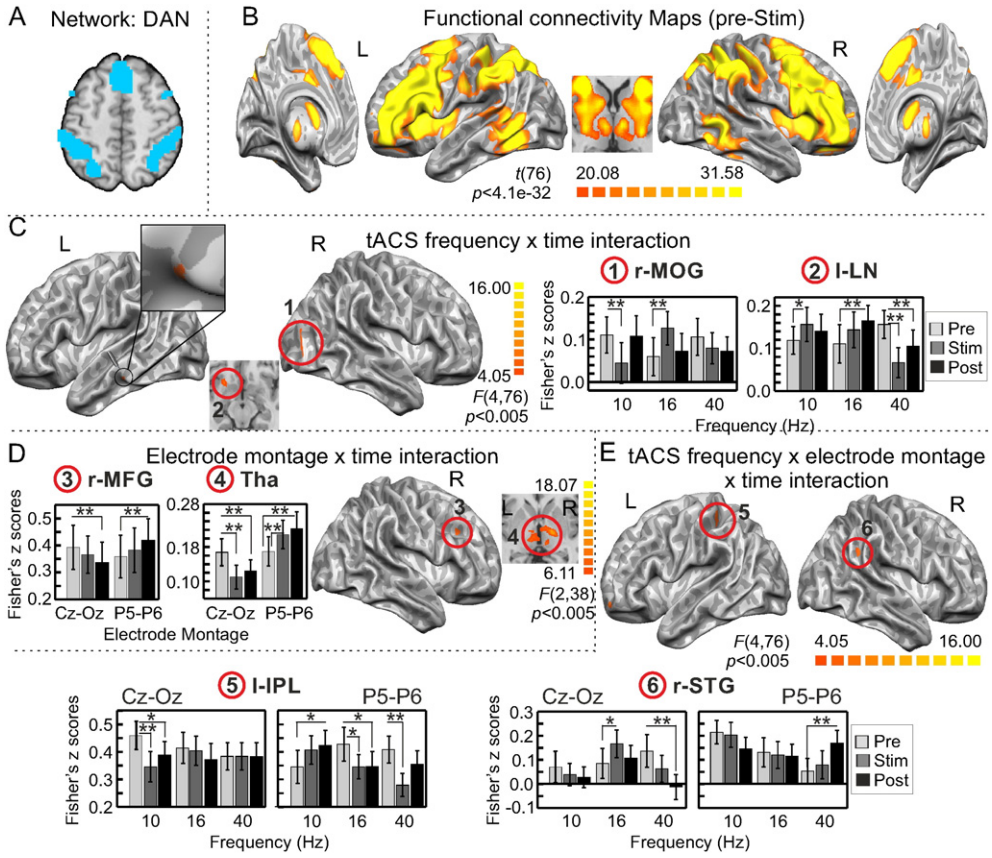

Fig. 5. Effect of tACS on functional connectivity relative to DAN. Significant interactions in the three-factor rANOVA performed on the DAN network-to-whole-brain functional connectivity analysis. A) Mask used for the DAN seed, B) Functional connectivity maps in the pre-stimulation conditions, C) tACS frequency × time interaction, D) Electrode montage × time interaction, E) tACS frequency × electrode montage × time interaction. Maps in C–E were thresholded using clusters determined by $p < 0.005$ and a corrected cluster significance threshold of $p < 0.05$. The resulting cluster size threshold was 9 functional voxels (243 mm) for C and 10 functional voxels (270 mm) for D and E. Bar graphs show post-hoc results for representative clusters for each interaction effect. Error bars denote standard error of the mean. L: left hemisphere, R: right hemisphere. MOG: middle occipital gyrus, LN: lentiform nucleus, MFG: middle frontal gyrus, Tha: thalamus, IPL: inferior parietal lobe, and STG: superior temporal gyrus. $^{*}p < 0.05$, $^{**}p < 0.01$.

40 Hz tACS decreased it both during and after the stimulation period. No significant electrode montage × time interaction was observed for this network. Significant tACS frequency × electrode montage × time interactions ($F(4, 76) > 4.05$, $p < 0.005$, Fig. 6D) were observed in a few clusters, including the right middle temporal gyrus (MTG) and CG. Post-hoc analyses showed that for the MTG, 10 Hz tACS decreased functional connectivity during and after the stimulation period when it was applied over Cz-Oz and increased functional connectivity during the stimulation period when applied over P5–P6. Stimulation with 16 Hz tACS decreased functional connectivity during the stimulation period only when it was applied over P5–P6. For the CG, 10 Hz tACS decreased functional connectivity during the stimulation over Cz-Oz. In addition, when tACS was applied over P5–P6, 16 Hz tACS increased functional connectivity after the stimulation period and 40 Hz decreased it during and post stimulation. A detailed description of the three-factor rANOVA and post-hoc results can be found in Supplemental materials, Table 4.

Similar to the DAN, tACS-induced modulation of functional connectivity between the l-FP and the whole brain was mainly observed in regions outside the network whose functional connectivity is low in the pre-stimulation periods. Spatially extensive tACS frequency × time interaction was observed between the l-FP and occipito-parietal regions, which matched our prediction of tACS modulating functional connectivity between regions close to the electrodes and more distant fronto-parietal areas.

Motor network. As for the networks described above, the correlation maps with the motor network seed (Fig. 7A) obtained in the pre-stimulation conditions (Fig. 7B) are similar to the original motor network component obtained from the ICA (compare Fig. 7B to Fig. 2A). Significant tACS frequency × time interaction ($F(4, 76) > 4.05$, $p < 0.005$, Fig. 7C) was observed in the left MFG and bilateral pulvinar nucleus in the thalamus. Post-hoc analyses showed that 10 Hz tACS increased functional connectivity between the motor network and both clusters, during the stimulation. This effect was observed in the post-stimulation period only for the pulvinar. The effect of 16 Hz tACS was observed as a decrease in functional connectivity between the motor network and the MFG during the stimulation and between the motor network and the pulvinar in the post-stimulation period. Stimulation with tACS at 40 Hz decreased functional connectivity only during the stimulation period for the MFG. Significant electrode montage × time interaction ($F(2, 38) > 6.11$, $p < 0.005$, Fig. 7D) was observed for the left SFG and the lingual gyrus (LingG). Post-hoc analyses showed that tACS decreased functional connectivity between the motor network and the left SFG only in the post-stimulation period when it was applied over Cz-Oz. For the LingG, tACS over Cz-Oz decreased functional connectivity during the stimulation period, while tACS over P5–P6 increased it both during and after the stimulation period. Significant tACS frequency × electrode montage × time interaction ($F(4, 76) > 4.05$, $p < 0.005$, Fig. 7E) was observed for several clusters, including the left insula and PoC. Interestingly, these two clusters are located within the motor network (Fig. 7B). For both clusters, and in agreement with the results obtained in the fALFF analysis, 10 Hz tACS increased functional connectivity during (PoC) and after (insula, PoC) the stimulation period when tACS was applied over Cz-Oz. Stimulation with 40 Hz tACS over Cz-Oz decreased functional connectivity during (insula) and after (insula, PoC) the stimulation period. When tACS was applied over P5–P6, 10 Hz tACS decreased functional connectivity in the post-

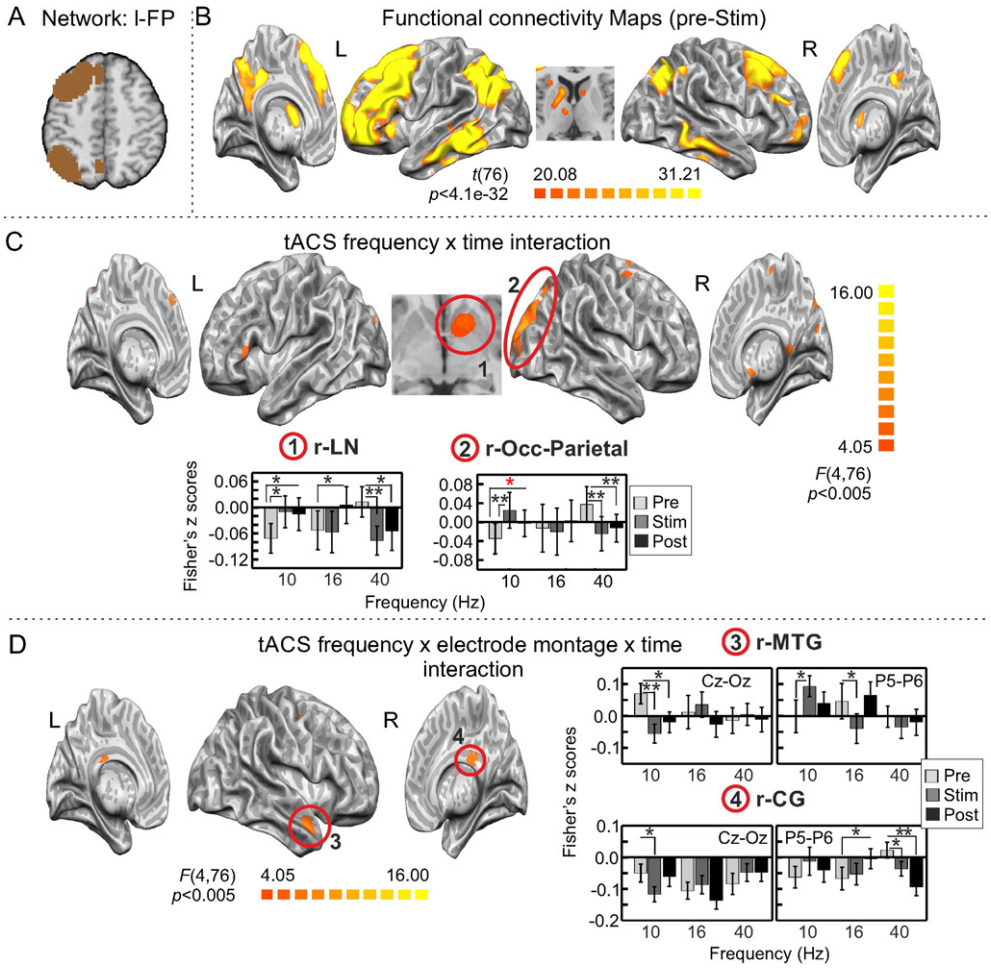

Fig. 6. Effect of tACS on functional connectivity relative to l-FP. Significant interactions in the three-factor rANOVA performed on the l-FP network-to-whole-brain functional connectivity analysis. A) Mask used for the l-FP seed, B) functional connectivity maps in the pre-stimulation conditions, C) tACS frequency × time interaction, D) tACS frequency × electrode montage × time interaction. Maps in C–D were thresholded using clusters determined by $p < 0.005$ and a corrected cluster significance threshold of $p < 0.05$. The resulting cluster size threshold was 13 functional voxels (351 mm) for C and 9 functional voxels (243 mm) for D. Bar graphs show post-hoc results for representative clusters for each interaction effect. Error bars denote standard error of the mean. L: left hemisphere, and R: right hemisphere. LN: lentiform nucleus, Occ: occipital, MTG: middle temporal gyrus, and CG: cingulate gyrus. Red* $p = 0.05$, * $p < 0.05$, ** $p < 0.01$.

stimulation period for both clusters while 16 Hz tACS decreased functional connectivity only for the PoC in the post-stimulation period. A detailed description of the three-factor rANOVA and post-hoc analyses is provided in Supplemental materials, Table 5.

In general, functional connectivity changes relative to the motor network resembled the pattern described in the previous section for the fALFF and for the other networks, with 10 and 40 Hz tACS showing opposite effects. Within-network functional connectivity changes were observed in insula and PoC.

Visual network. Correlation maps in the pre-stimulation conditions resemble closely the original component representing the visual network obtained with ICA (Figs. 8A–B, compare Fig. 8B to Fig. 2A). Significant tACS frequency × time interaction ($F(4, 76) > 4.05$, $p < 0.005$, Fig. 8C) was found for a few clusters, including the PCC and the left MOG. Post-hoc analyses showed that the visual network functional connectivity to both clusters increased with 10 Hz tACS during and after (only PCC) the stimulation period. Stimulation with tACS at 16 Hz increased functional connectivity between the visual network and the PCC after the stimulation and decreased functional connectivity between the visual network and the MOG during and after the stimulation. Stimulation with tACS at 40 Hz decreased functional connectivity between the visual network and the PCC after the stimulation period. Note that the MOG cluster belongs to the visual network, given by high correlation values between the visual network and this cluster in the pre-stimulation condition (Fig. 2A, Fig. 8B). Significant electrode montage × time interaction ($F(2, 38) > 6.11$, $p < 0.005$, Fig. 8D) was found for a few clusters, including the left insula and the right IFG. Post-hoc analyses showed that Cz-Oz stimulation increased functional connectivity between the visual network and the insula while P5–P6 decreased this relationship during stimulation. In terms of electrode montage, Cz-Oz tACS also decreased visual network correlation with IFG in the post-stimulation period. A significant tACS frequency × electrode montage × time interaction ($F(4, 76) > 4.05$, $p < 0.005$, Fig. 8E) was found for left MFG and in a cluster intersecting middle and superior frontal gyri (MFG/SFG). The visual network correlation with MFG/SFG was affected only when tACS was applied over P5–P6, with 10 Hz increasing this functional connectivity during the stimulation period, and 16 and 40 Hz decreasing it during and after (only for 40 Hz) the stimulation. The functional connectivity between the visual network and the MFG increased with 10 Hz tACS over Cz-Oz in the post-stimulation period and decreased with 40 Hz tACS over Cz-Oz during the stimulation. Stimulation with 16 Hz tACS decreased functional connectivity between the visual network and the MFG during the stimulation period, when it was applied over P5–P6. A detailed description of the three-factor rANOVA and post-hoc results is provided in Supplemental materials, Table 6.

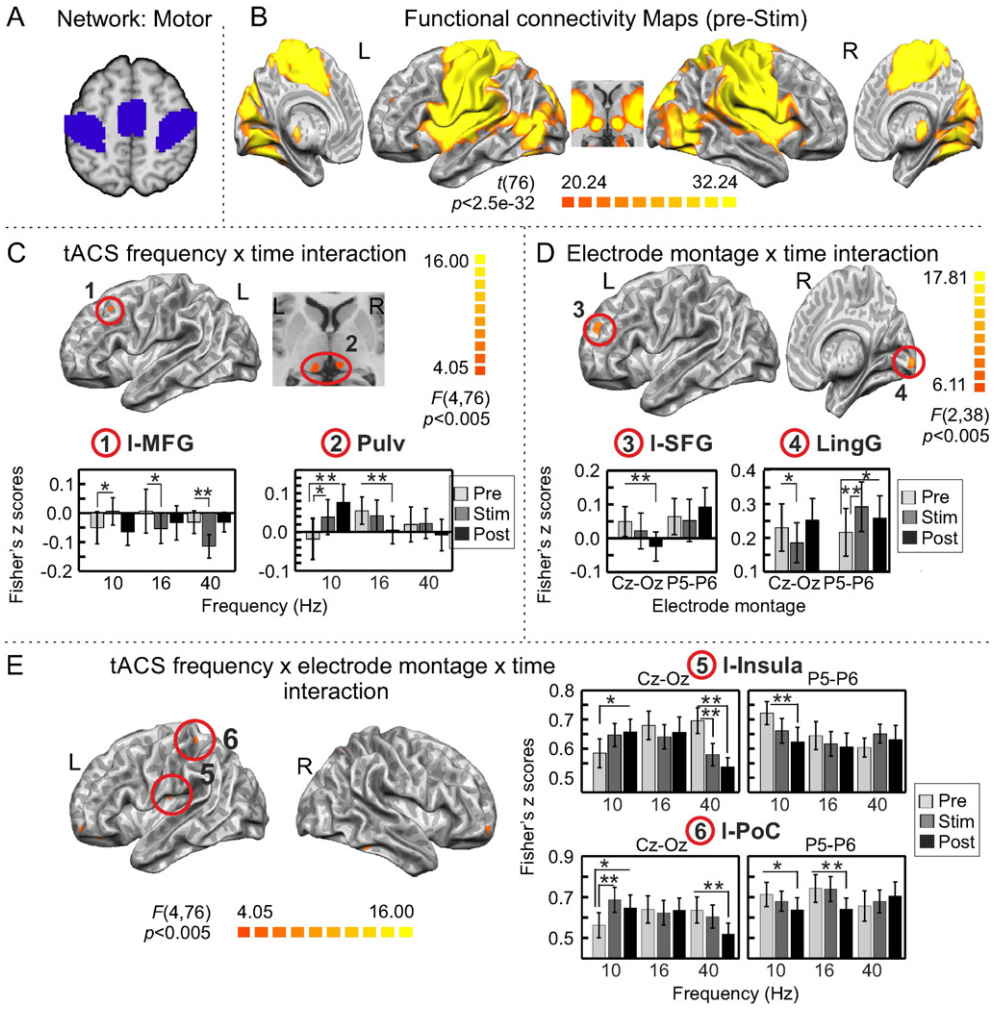

Fig. 7. Effect of tACS on functional connectivity relative to motor network. Significant interactions in the three-factor rANOVA performed on the motor network-to-whole-brain functional connectivity analysis. A) Mask used for the motor network, B) functional connectivity maps in the pre-stimulation conditions, C) tACS frequency × time interaction, D) electrode montage × time interaction, E) tACS frequency × electrode montage × time interaction. Maps in C–E were thresholded using clusters determined by $p < 0.005$ and a corrected cluster significance threshold of $p < 0.05$. The resulting cluster size threshold was 10 functional voxels (270 mm) for C and E, and 9 functional voxels (243 mm) for D. Bar graphs show post-hoc results for representative clusters for each interaction effect. Error bars denote standard error of the mean. L: left hemisphere, R: right hemisphere. MFG: middle frontal gyrus, Pulv: pulvinar, SFG: superior frontal gyrus, LingG: lingual gyrus, and PoC: postcentral gyrus. $^{*}p < 0.05$, $^{**}p < 0.01$.

In summary, functional connectivity changes relative to the visual network were mainly observed between this network and regions outside of the network, except for the MOG, and followed the previously described pattern of 10 and 40 Hz tACS showing opposite effects.

Overall, results from the seed-based functional connectivity analyses using the selected RSNs showed that tACS effects on RSN functional connectivity were frequency- and electrode montage-dependent, with 10 and 40 Hz tACS often inducing opposite sign of effects. Most of the tACS effects were observed as modulation of *inter*-network functional connectivity (as observed in network-to-network and network-to-whole-brain correlations). *Intra*-network functional connectivity changes were observed for the DAN (IPL), the motor network (insula, PoC) and the visual network (MOG). The l-FP showed the most extensive frequency-dependent modulation in functional connectivity, mainly with occipito-parietal areas.

tACS-induced changes in functional connectivity relative to maximally stimulated areas

Apart from assessing intrinsic resting-state networks, another important question is whether tACS modulates functional connectivity between directly stimulated and distant brain regions. This analysis would help explain results from our previous study showing that tACS modulated the BOLD signal in regions distant from the electrodes. To this end, three different ROIs were generated based on the regions with the highest electric field across subjects (Oz, P5, P6, see Methods) as predicted by simulations (Fig. 3, Fig. S2). These ROIs were employed as seeds for seed-based functional connectivity analyses, wherein each seed's average time course was correlated with that of every other voxel in the brain (Supplemental materials, Fig. S2 C).

For tACS over Cz-Oz, the seed (Oz) region was located within the occipital cortex (Fig. 9A, Supplemental materials, Fig. S1). The group functional connectivity map of the pre-stimulation conditions shows that this seed exhibits greatest functional connectivity with other regions within the occipital cortex (Fig. 9B), constituting a network that resembles the visual network component obtained with our ICA analysis (compare Fig. 9B to Fig. 2A). This suggests that, based on the electric field simulations, tACS over Cz-Oz maximally stimulates the visual network. To evaluate whether tACS over Cz-Oz modulates functional connectivity of the area directly stimulated (as predicted by our electric field simulations), a two-factor rANOVA evaluating tACS frequency × time interaction effects was conducted with the data collected when tACS was applied with the Cz-Oz montage. Significant tACS frequency × time interaction ($F(4, 76) > 4.05$, $p < 0.005$, Fig. 9C) was observed within the network in the left Cu, but mainly in regions outside of the visual network, including the left MedialFG and insula.

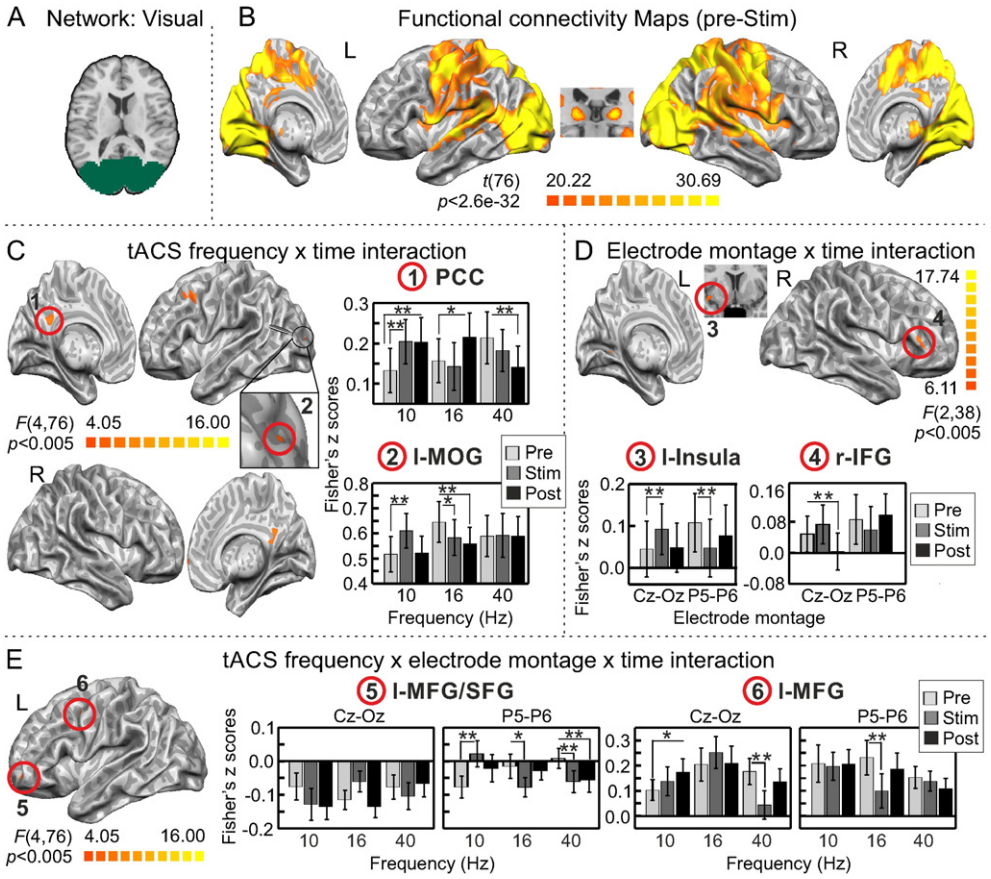

Fig. 8. Effect of tACS on functional connectivity relative to the visual network. Significant interactions in the three-factor rANOVA performed on the visual network-to-whole-brain functional connectivity analysis. A) Mask used for the visual network seed, B) functional connectivity maps in the pre-stimulation conditions, C) tACS frequency × time interaction, D) electrode montage × time interaction, E) tACS frequency x electrode montage x time interaction. Maps in C-E were thresholded using clusters determined by $p < 0.005$ and a corrected cluster significance threshold of $p < 0.05$. The resulting cluster size threshold was 11 functional voxels (297 mm) for C, 9 functional voxels (243 mm) for D, and 10 functional voxels (270 mm) for E. Bar graphs show post-hoc results for representative clusters for each interaction effect. Error bars denote standard error of the mean. L: left hemisphere, R: right hemisphere. PCC: posterior cingulate cortex, MOG: middle occipital gyrus, IFG: inferior frontal gyrus, MFG: middle frontal gyrus, and SFG: superior frontal gyrus. $^{*}p < 0.05$, $^{**}p < 0.01$.

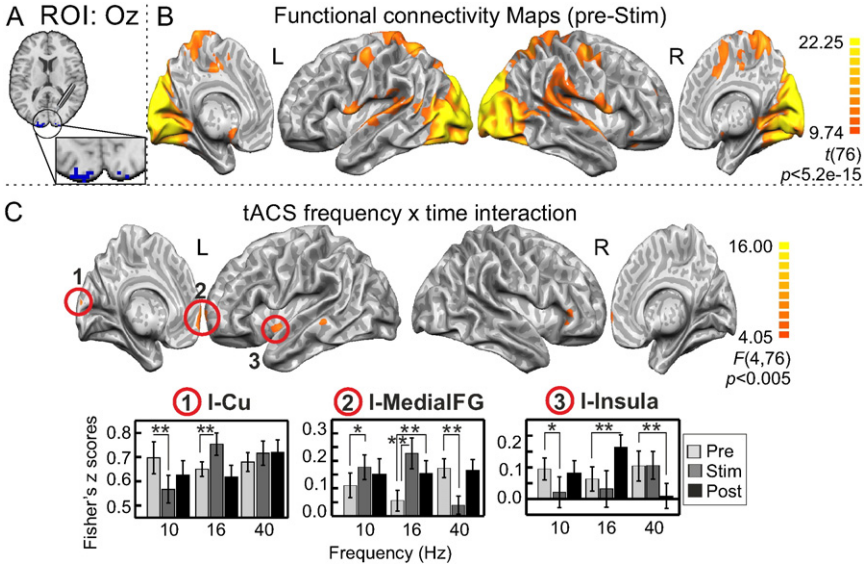

Fig. 9. Effect of tACS on functional connectivity relative to simulation-based ROI Oz. Significant interactions in the two-factor rANOVA performed on the Oz functional connectivity analysis. A) Mask used for the Oz seed, B) Functional connectivity maps in the pre-stimulation conditions, C) tACS frequency x time interaction. Maps in C were thresholded using clusters determined by $p < 0.005$ and a corrected cluster significance threshold of $p < 0.05$. The resulting cluster size threshold was 11 functional voxels (297 mm). Bar graphs show post-hoc results for representative clusters for the interaction effect. Error bars denote standard error of the mean. L: left hemisphere, R: right hemisphere. Cu: cuneus, and MedialFG: medial frontal gyrus. $^{*}p < 0.05$, $^{**}p < 0.01$.

Post-hoc analyses showed that 10 Hz tACS was most effective during the stimulation period, significantly decreasing functional connectivity between the Oz seed and the Cu as well as the insula, and increasing it with the MedialFG. Stimulation with tACS at 16 Hz increased functional connectivity between the seed and these three regions, which was observed during (Cu) or after (insula) the stimulation period, or both (MedialFG). On the other hand, 40 Hz tACS mainly decreased functional connectivity between the seed and regions outside the visual network during or after the stimulation period. For a more detailed description of the results, please refer to Supplemental materials, Table 7.

Continuing with the electric field simulation-based seeds, for tACS over P5–P6, one seed region was situated in the posterior parietal cortex in each hemisphere (P5, P6) (Supplemental materials, Fig. S1). Two-factor rANOVAs were conducted separately for the P5 and P6 seeds, including only the conditions with stimulation applied over P5–P6 in order to test whether this montage was able to induce changes in the functional connectivity of the regions being maximally stimulated. For the P5 seed (Fig. 10A), the group functional connectivity map of the pre-stimulation conditions shows greatest functional connectivity between this seed and fronto-parietal regions, which is more pronounced in the left hemisphere (Fig. 10B). This functional connectivity map resembles the l-FP component obtained with our ICA analysis (compare Fig. 10B to Fig. 2A). A significant tACS frequency × time interaction ($F(4, 76) > 4.05$, $p < 0.005$, Fig. 10C) was observed in several clusters, including right Cu and LN. Post-hoc analyses showed that in most of the clusters, as already reported for previous analyses, 10 and 40 Hz tACS induced opposite effects, with 10 Hz tACS mainly increasing functional connectivity (during and/or after the stimulation period) and 40 Hz tACS decreasing it (mainly after the stimulation period). Note that similar clusters (i.e., Cu and LN) exhibited the same functional connectivity modulation in the P5 seed analysis and l-FP network-to-whole-brain functional connectivity analysis (compare Fig. 10C to Fig. 6C). Most changes in functional connectivity relative to the P5 seed (left hemisphere) were observed in regions in the right hemisphere, suggesting tACS modulation of inter-hemispheric functional connectivity, as shown in EEG-tACS studies (Helfrich et al., 2014b). For a more detailed description of the results, please refer to Supplemental materials, Table 8.

Stimulation with tACS was less effective at modulating the functional connectivity with the P6 seed, whose functional connectivity map in the pre-stimulation condition resembles that of the r-FP (compare Supplemental materials Fig. S6 to Fig. 2A). A significant tACS frequency × time interaction ($F(4, 76) > 4.05$, $p < 0.005$) was found only for the right SFG, where 10 and 40 Hz tACS induced opposite effects in the post-stimulation period. Note that no inter-hemispheric functional connectivity changes were observed for P6.

Overall, using electric field simulation-based seed correlations, we observed that tACS over Cz-Oz and P5–P6 maximally stimulate different networks, with stimulation over Cz-Oz targeting the visual network and stimulation over P5–P6 targeting left and right fronto-parietal control networks. As expected, tACS modulated functional connectivity between directly stimulated regions and areas distant from the electrodes. However, no significant functional connectivity changes were observed between the Oz seed and fronto-parietal areas, contrary to our expectations based on the results from our previous tACS-fMRI study (Cabral-Calderin et al., 2016). The effects of tACS over P5–P6 on functional connectivity with the left seed (P5) were more pronounced than with the right seed (P6).

In the present study, we reported only frequency- or/and electrode montage-dependent effects of tACS. Additional analyses evaluating non-specific tACS effects suggested that the effects of tACS on fALFF and functional connectivity were mostly frequency dependent and that non-specific effects were minimal (see Supplemental materials, Results and Fig. S7).

Phosphene perception, cutaneous sensation and fatigue ratings

We evaluated sensory and fatigue experience ratings related to tACS at each frequency and with each electrode montage. The three-factor rANOVA showed a significant tACS frequency × time interaction on the phosphene perception ratings ($F(4, 76) > 3.78$, $p = 0.007$, Supplemental materials, Fig. S8). As already described in the literature, post-hoc analyses showed a significant increase in the phosphene ratings during 10 and 16 Hz tACS ($p = 0.01$ and $p < 0.001$, respectively, (Kanai et al., 2008; Turi et al., 2013)). Stimulation with tACS at 40 Hz did not induce phosphene perception. No significant electrode montage × time interaction or tACS frequency × electrode montage × time interaction was observed for the phosphene ratings. No significant interactions were observed for the cutaneous sensation and the fatigue ratings. Overall, these analyses showed that 10 and 16 Hz tACS induced phosphenes with a similar strength while 40 Hz tACS did not induce

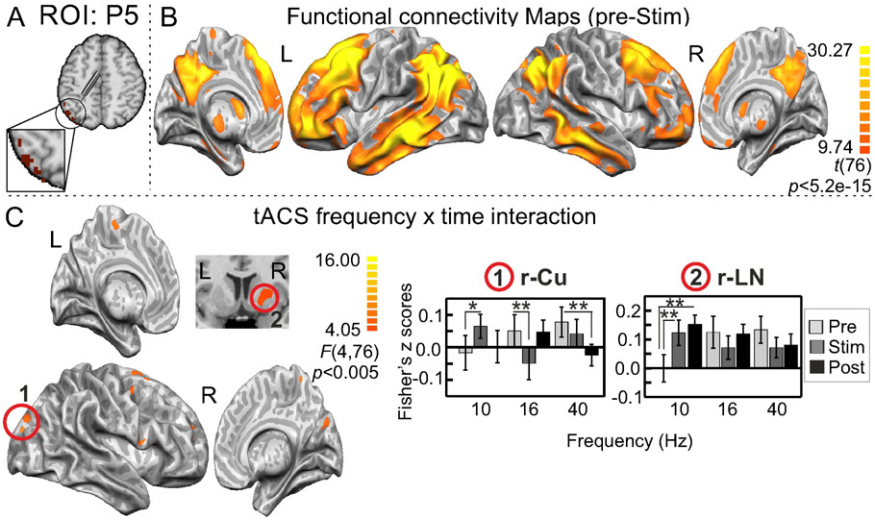

Fig. 10. Effect of tACS on functional connectivity relative to simulation-based ROI P5. Significant interactions in the two-factor rANOVA performed on the P5 functional connectivity analysis. A) Mask used for the P5 seed, B) functional connectivity maps in the pre-stimulation conditions, C) tACS frequency × time interaction. Maps in C were thresholded using clusters determined by $p < 0.005$ and a corrected cluster significance threshold of $p < 0.05$. The resulting cluster size threshold was 12 functional voxels (324 mm). Bar graphs show post-hoc results for representative clusters for the interaction effect. Error bars denote standard error of the mean. L: left hemisphere, R: right hemisphere. Cu: cuneus, and LN: lentiform nucleus. $^{*}p < 0.05$, $^{**}p < 0.01$.

significant phosphene perception. Subjects perceived the stimulation with similar discomfort across frequencies and electrode montages.

In order to evaluate the impact of tACS-induced sensory experiences on spontaneous low frequency BOLD signal fluctuations, the individual phosphene perception and cutaneous sensation ratings were correlated to the individual mean fALFF values extracted from sample ROIs located in primary visual (V1) and somatosensory (S1) cortices, respectively (Supplementary materials). Four ROIs were created by defining a 7 mm radius sphere around the center of Brodmann area 17 (for V1) and Brodmann areas 1–3 (for S1), for each hemisphere. We hypothesized that any effect of tACS-induced sensory experiences should be largest in the corresponding primary sensory cortices. No significant correlation was observed between the fALFF and either phosphene perception (mean p-value across comparisons: $p = 0.547$, *range* 0.089–0.916) or somatosensory ratings (mean p-value across comparisons: $p = 0.535$, *range* 0.122–0.974) during tACS stimulation for any ROI. Note that, overall, participants rated phosphene perception and cutaneous sensation with low intensities (mean values ranged from 1 to 2.25 (on a scale of 1–10)), probably due to the long stimulation times. Sensory experiences with higher intensities could have a different impact on fALFF values in primary cortices.

Discussion

In the present study, we investigated the effects of tACS on spontaneous low frequency BOLD signal fluctuations, a measure that allows characterization of RSNs. The practice of using resting-state functional connectivity to inform brain stimulation targets is increasingly gaining attention in the quest for effective brain stimulation methods (Opitz et al., 2015a; Fox et al., 2014; Fox et al., 2012). The focus of the discussion will be on the most significant and stable findings across the different analysis approaches rather than every specific result. The electric field simulations showed that tACS over Cz-Oz mainly stimulates the occipital cortex, while tACS over P5–P6 primarily stimulates parietal cortices. As partly predicted from previous behavioral/imaging studies (Feurra et al., 2011a; Kanai et al., 2008; Alekseichuk et al., 2015; Cabral-Calderin et al., 2016; Raco et al., 2014; Feurra et al., 2011b), tACS effects were frequency and partially electrode montage dependent. In regions where frequency-dependent effects of tACS were observed, 10 and 40 Hz tACS generally induced opposite effects. Most tACS effects were observed as modulation of inter-network functional connectivity (e.g., l-FP to visual network, l-FP to DMN). Intra-network functional connectivity changes were observed only in a few clusters within DAN (IPL), motor network (insula, PoC) and visual network (MOG). The l-FP showed the most extensive frequency-dependent modulation in functional connectivity, mainly with occipito-parietal regions. Taken together, our results show that tACS is able to modulate local spontaneous low frequency fluctuations and their correlations with distant regions, which should be taken into account when interpreting tACS effects on brain function.

Effects of tACS as predicted by the electrode montages and electric field simulations

Using electric field-based seeds predicted by FEM model simulations, we showed that tACS over Cz-Oz is most likely to maximally stimulate the visual network while over P5–P6 it targets left and right fronto-parietal control networks (Neuling et al., 2012). Further analyses showed that most electrode-dependent effects were given by opposite sign of effects induced by tACS with each electrode montage, though both montages affected similar regions, at least to some extent. It is important to note that, although the maximum electric field for each montage was located in different regions, given the spatial proximity of the two electrode montages, lower electric fields from the individual simulations that did not pass the 50% masking threshold share common brain regions, primarily in medial occipito-parietal areas. This suggests that, even though each electrode montage strongly targets a particular network, part of the applied current could still extend to regions common to both montages. More focal montages (e.g., high-density montages) might induce more specific montage-dependent effects. The opposite effects of electrode montage could arise from the fact that, with our electrode montages, tACS stimulation is antiphase (i.e., 180° phase difference between the two stimulated sites (Polania et al., 2012; Struber et al., 2014)). With tACS over Cz-Oz, posterior regions are stimulated with a 180° phase difference with respect to each electrode, however, stimulation is hemispherically symmetric along the midline. A different pattern is induced by tACS over P5–P6, where the hemispheres are stimulated with a 180° phase difference. However, the goal of the present study was not to compare inter-hemispheric functional connectivity changes, but to analyze tACS modulation in the context of resting-state networks, which are typically bilaterally defined (Fox et al., 2005; Beckmann et al., 2005). In addition, we aimed to examine changes relative to directly stimulated sites, which are also not constrained to single hemispheres in this study. Inferences about inter-hemispheric functional connectivity could perhaps be made with our electric field simulation-based seeds for tACS over P5–P6. Here, seeds were unilaterally placed over parietal areas in each hemisphere, although it is important to note that though the seeds are separated into hemispheres, the stimulation was not. Stimulation with tACS over P5–P6 might be more likely to induce changes in functional connectivity between hemispheres than Cz-Oz tACS because, as mentioned above, each hemisphere is stimulated with a 180° phase relationship to the other, in contrast to the Cz-Oz montage. In a previous tACS-EEG study, it was shown that 40 Hz tACS applied with a similar montage (~P7–P8) impaired interhemispheric functional coupling observed as a decrease in the interhemispheric EEG coherence (Helfrich et al., 2014b). Therefore, we would expect to observe decreases in functional connectivity between corresponding areas in both hemispheres. In agreement with that prediction, we observed that 40 Hz tACS decreased functional connectivity between the left parietal seed (P5) and several clusters in the right hemisphere, including the right cuneus. However, induced modulation was frequency dependent, with 10 Hz causing the opposite effect, i.e., increased functional connectivity between the P5 seed and the right cuneus. Therefore, a direct link to inter-hemispheric coupling impairments due to anti-phasic stimulation cannot be made. In their study, Helfrich et al. (2014b) evaluated tACS effects in interhemispheric EEG coherence only for tACS at 40 Hz; whether the same pattern should be observed for other tACS frequencies still needs to be established. Future studies could expand on inter- vs. intra-hemispheric changes in functional connectivity by directly comparing in-phase vs. anti-phase montages over the same regions with the same frequencies. Although the present study was not aimed at evaluating how individual differences affect tACS effects, the inclusion of the electric field strength information in the fALFF analysis suggested that incorporating individual predictions based on electric field simulations could be a valuable approach for evaluating tACS effects in both neural and behavioral studies.

Opposite effects of 10 and 40 Hz tACS

One main finding of this study was that in most of the analyzed networks, 10 Hz tACS increased functional connectivity while 40 Hz tACS decreased it, or vice versa. This is in line with the opposite effects of 10 Hz and 40 Hz stimulation on local activity as determined by fALFF analysis. The antagonism between alpha and gamma frequencies has been well documented in the literature, suggesting that alpha power is more related to idling brain state and functional inhibition of task-irrelevant regions (Jensen and Mazaheri, 2010; Spaak et al., 2012) while gamma oscillations are more related to the performance of perceptual and cognitive operations (Tagliazucchi et al., 2012; Spaak et al., 2012). Different conceptions of neural activity could be related to this antagonism of 10 and 40 Hz tACS. First, there is evidence that

during visual processing, alpha oscillations are related to feedback projections and gamma oscillations are more related to feedforward mechanisms (Tagliazucchi et al., 2012; Spaak et al., 2012; Jensen et al., 2015). Second, alpha oscillations have been related to information transmission across long-distance areas while gamma oscillations are associated with local cortical assemblies (von Stein and Sarnthein, 2000). Third, it has been shown that alpha and gamma oscillations relate to each other via cross-frequency coupling (e.g., phase-amplitude coupling or amplitude-envelope correlations) (Canolty and Knight, 2010; Helfrich et al., 2015). For example, recent studies reported no modulation of gamma power but reduced alpha power due to gamma tACS entrainment (Helfrich et al., 2014b; Helfrich et al., 2015). According to this, our results could be explained by opposite modulations of alpha power, i.e., tACS at 10 Hz increased alpha power (Helfrich et al., 2014a; Helfrich et al., 2015) while tACS at 40 Hz decreased alpha power via cross-frequency coupling (Helfrich et al., 2014b; Helfrich et al., 2015). However, given the nature of our study (low frequency measurement without concurrent electrophysiological measurements), sound conclusions about cross-frequency coupling cannot be made.

The effects of tACS were not always as predicted for the different combinations of tACS frequencies and electrode montages used in our study. For instance, for each electrode montage, tACS effects were not limited to the directly stimulated regions. In addition, the effects of a given frequency were not always as expected according to the existent literature linking brain oscillations to RSNs (Tagliazucchi et al., 2012; Mantini et al., 2007; Mo et al., 2013; Zhan et al., 2014; Scheeringa et al., 2012). A particular example is the observed effect induced by tACS at 10 Hz. Contrary to our expectations, we found that, in some brain regions, 10 Hz tACS increased functional connectivity with particular RSNs rather than decreased it. Examples of this pattern are the increase in functional connectivity of the l-FP with occipito-parietal regions and LN as well as the increase in functional connectivity of the visual network with MOG. This finding is reminiscent of findings in our previous study (Cabral-Calderin et al., 2016) where short periods (30 s) of tACS at alpha and beta frequencies mainly increased BOLD signal amplitude in fronto-parietal areas.

These results are surprising if one takes into account the vast literature suggesting that the BOLD signal at rest is mainly negatively correlated to alpha oscillations and positively linked to gamma rhythms. One important aspect to take into account is the relationship between oscillatory entrainment and the BOLD signal, which is not well understood (Muthukumaraswamy and Singh, 2009; Parkes et al., 2004). Previous EEG studies have found that alpha tACS increased alpha power in occipito-parietal areas (Helfrich et al., 2014a; Neuling et al., 2013), however, whether or not these power increases observed in the EEG are translated the same way into the BOLD signal is not clear. It might be that the online entrainment induced by tACS does not impose a change in the metabolic demand of the entrained brain area, therefore the expected change in the spontaneous activity induced by alpha or gamma tACS may not be observed during the stimulation period with fMRI. Note that the apparent discrepancy between the results from this study and our previous study, and the previously reported negative correlation between alpha power and BOLD signal relies on the assumption that 10 Hz tACS increased alpha power (Helfrich et al., 2014a; Neuling et al., 2013). However, since we did not measure concurrent electrophysiological data, we cannot be certain about the latter. A recent study showed that one second of alpha tACS did not produce aftereffects in amplitude or phase of the EEG signals (Struber et al., 2015). Along those lines, it could be that short stimulation periods of 10 Hz tACS are not enough to increase alpha power, which would explain the lack of negative association between 10 Hz tACS and the BOLD signal in our previous study, where tACS was applied only for 30 s (Cabral-Calderin et al., 2016). Moreover, the effect of tACS is task-dependent and increase in alpha power seems to depend on brain state (Neuling et al., 2013). Therefore, increased alpha power resulting from 10 Hz tACS, however likely, cannot always be assumed. Further research is needed to work out the mechanisms that led to the observed effects of tACS in fALFF and functional connectivity.

Across the different analyses, we did not observe a clear pattern distinguishing between online and after-effects of tACS. The effects of tACS were observed either as changes in functional connectivity during the stimulation that outlasted stimulation or returned to non-significant levels in the post-stimulation period, or as changes in functional connectivity only in the post-stimulation period. Differences between online and after-effects of tACS might be explained by different dynamic mechanisms, i.e., online changes could reflect oscillatory entrainment while after-effects could be related to changes in plasticity (Vossen et al., 2015).

As previously mentioned in the results, one possible confound in any tACS study is that the observed changes induced by stimulation could reflect sensory experiences rather than tACS entrainment (Schutter, 2015; Kar and Krekelberg, 2012). It has been shown that tACS induces phosphene perception and cutaneous sensation in a frequency-dependent manner (Kanai et al., 2008; Turi et al., 2013). We did not find any significant difference in somatosensory ratings between the different frequencies. In addition, although gamma tACS induced less phosphene perception, ratings for tACS at alpha and beta frequencies were similar. If one assumes that tACS effects in our study are related to phosphene perception, one would expect to observe similar effects with 10 and 16 Hz tACS because they induced phosphene perception with a similar strength in our participants. However, this was not the case for most results reported here. Moreover, if tACS-induced sensory experiences affect spontaneous fMRI signal fluctuations, we expect this effect to be maximal in the corresponding primary sensory cortices. However, the during-stimulation fALFF values extracted from specific ROIs within the primary visual and somatosensory cortices did not show a significant correlation with phosphene perception or somatosensory ratings, respectively, for any tACS frequency for any electrode montage. Based on our results, we assume that sensory experiences are unlikely to account for the here reported changes in fALFF or functional connectivity. These findings are also in agreement with our previous study where no significant association between cutaneous sensation, phosphene perception ratings and tACS-induced modulation in the BOLD signal was observed during eyes-open conditions (Cabral-Calderin et al., 2016). Nonetheless, it is worth mentioning that, similar to our previous study (Cabral-Calderin et al., 2016), participants rated their subjective phosphene perception and cutaneous sensation intensities. We cannot entirely exclude that unconsciously perceived phosphenes induced secondary effects such as attention shifts (Brignani et al., 2013).

Effects of tACS as a modulation of inter-network functional connectivity

Most of the effects found in this study were changes in functional connectivity between networks or regions belonging to different RSNs. Exceptions from this rule were changes in a few clusters within the DAN, motor and visual networks. It is possible that our network-based analysis might be biased to detect functional connectivity changes between the given RSN and areas outside of the seed, and that smaller within-network node ROIs or voxel-wise analyses might be more suitable for detecting within-network changes. However, the analysis with electric field simulation-based ROIs, in which a smaller seed was used as reference for functional connectivity maps, did not show additional within-network changes. We thus believe that during resting conditions, tACS is more likely to modulate functional connectivity between than within networks. One could speculate that changes in functional connectivity due to tACS are more easily induced between areas in which reciprocal functional connectivity is weak, while a higher energy level might be required for modulating strong functional connectivity. Previous studies suggested that the lack of effect with non-invasive brain stimulation methods could be explained by a ceiling effect (Neuling et al., 2013; Salomons et al., 2014; Nettekoven et al., 2015).

In our case, "ceiling effect" could be defined in terms of either ongoing oscillations or the BOLD signal itself. In other words, it could be that the amplitude of the oscillations at the applied frequency was already at (or close to) a maximum value (Ehm et al., 2011), therefore no further enhancement is observed with tACS. Another possibility is that the metabolic demands of some functional networks were already optimally driven, and therefore these networks are not driven more by electrical stimulation (Ekstrom et al., 2008). A particular example of this could be the lack of tACS effect in the fALFF and functional connectivity analysis with the DMN. The DMN is a task-negative network that has been reported to be most active in resting conditions; therefore, we hypothesize that already strongly activated networks/regions that exhibit high functional and anatomical connectivity cannot be modulated more with tACS. This point of view would be in agreement with our previous study where we showed that the effect of tACS during motor or visual task conditions was mainly observed in regions not activated by the task (Cabral-Calderin et al., 2016). Along the same lines, a previous EEG study showed that tACS-entrainment only occurred when the intrinsic power at this frequency was present, but relatively low (Neuling et al., 2013).

Left fronto-parietal control network: a particularly vulnerable candidate?

One of the networks showing strongest modulation in its functional connectivity was the left fronto-parietal control network (l-FP), which showed tACS-induced changes in functional connectivity in the network-to-network and network-to-whole-brain functional connectivity analyses, and it was also found to be modulated when the P5 seed from the electric field simulation was analyzed. The most extensive frequency-dependent modulation in functional connectivity relative to the l-FP was observed in occipito-parietal regions, where 10 Hz tACS increased and 40 Hz tACS decreased correlation values. This result is reminiscent of our previous study showing stronger tACS-induced increases in BOLD signal in left fronto-parietal regions (Cabral-Calderin et al., 2016). One possibility is that tACS is most effective in particular cortical regions because of vulnerability brought on by metabolic energy compromises that must take place in regions that play multiple roles or act as functional hubs but have not evolved high efficiency (Tomasi et al., 2013). A study modeling the relationship between glucose metabolism, measured with fludeoxyglucose in positron emission tomography, and resting-state functional connectivity found higher metabolism associated with higher rs-fMRI signal amplitudes in the cerebellum, occipital cortex, and parietal cortices relative to the rest of the brain. However, the same study showed that glucose efficiency in cerebellum, thalamus, and other subcortical structures is higher than in the cortex. Thus, it could be postulated that functional hubs like in the fronto-parietal networks would be particularly susceptible to any manipulation that challenges energy consumption (Tomasi et al., 2013). Fronto-parietal regions play multiple functional roles involved in facilitating attention, language, memory, and visual consciousness (Naghavi and Nyberg, 2005; Zhu et al., 2014). In functional connectivity studies, fronto-parietal networks are considered as control networks found to mediate DAN-DMN anticorrelations in a task-dependent manner (Gao and Lin, 2012; Spreng et al., 2013). In fact, the left fronto-parietal control network seems particularly susceptible to perturbations and has been shown to break down in neurological diseases such as Lewy body dementia (Peraza et al., 2015) and aphasic stroke (Zhu et al., 2014), in which the degree of network disruption is associated with the deficit's severity and recovery. In addition, previous studies have shown modulation of the amplitude of the BOLD signal or functional connectivity of fronto-parietal regions due to tACS or transcranial magnetic stimulation, respectively (Cabral-Calderin et al., 2016; Gratton et al., 2013). The flexibility of the left fronto-parietal control network might explain its sensitivity to tACS modulation.

We previously showed that tACS over Cz-Oz increased the BOLD signal in fronto-parietal regions (most strongly in the left hemisphere) but not in the areas close to the electrodes, such as occipital cortex (Cabral-Calderin et al., 2016). We hypothesized that this modulation of distant areas could be explained by changes in functional connectivity between these areas and the directly stimulated regions. In the present study, we found that the functional connectivity between the l-FP (which includes the regions reported in our previous study, such as MFG and IPL) and occipital regions was modulated by tACS in a frequency-dependent manner. These results partially match our previous hypothesis. However, when the seed region for the functional connectivity analysis was placed over Oz (for tACS over Cz-Oz), which would match our previous design, no significant functional connectivity changes were observed with similar fronto-parietal areas. We would like to point out, however, that our seed region for Oz only included the voxels where the strongest electric field was observed for most of the subjects and not the entire stimulated area. It could still be possible that stimulated areas outside our Oz seed are changing functional connectivity with the left fronto-parietal control network. Results from this and our previous study suggest that the l-FP is a network that is easy to perturb with tACS. Future studies could expand on the possibility of using tACS for modulating l-FP functional connectivity in patient populations where decreased l-FP functional connectivity has been reported (Zhu et al., 2014; Peraza et al., 2015).

Implications for behavioral studies

We previously showed that tACS effects on the BOLD signal were not typically observed in the areas under the electrodes but mainly in more distant fronto-parietal regions (Cabral-Calderin et al., 2016). In agreement with those findings, the present study showed that tACS effects are not limited to the directly stimulated brain regions, i.e., tACS also modulates spontaneous BOLD signal fluctuations in distant regions (e.g., medial frontal gyrus) as well as functional connectivity between spatially distant networks/regions (e.g., between the l-FP and the visual network). These results suggest that tACS effects are influenced by network interactions, which should be considered when interpreting behavioral effects of tACS. Behavioral consequences of tACS cannot be interpreted based only on the role of the directly stimulated regions, and the roles of functional networks should also be considered. For instance, when applying tACS over the occipital cortex, the logical aim is to modulate the activity in visual areas, and, in consequence, the performance in a given visual task. However, our results suggest that using this stimulation protocol, the activity of fronto-parietal areas – as well as their functional connectivity with more distant brain regions – is also being modulated. Therefore, any change in visual task performance could be influenced by attentional or executive control processes, more than by local changes in visual areas. However, it is important to note that the results shown in the present study pertain to resting-state conditions. Since tACS effects on the BOLD signal are strongly task dependent (Cabral-Calderin et al., 2016), inference from resting state to task-related tACS effects should be made carefully. Future studies could evaluate functional connectivity changes induced by tACS under the task condition of interest, e.g., with fMRI or electrophysiological measurements cleared from tACS-induced artifacts, and implement causational analysis techniques like psychophysiological interactions or dynamic causal modeling.

Limitations

Resting-state functional connectivity in a single subject varies over time (Chang and Glover, 2010; Hutchison et al., 2013). In addition, some studies reported the effect of stimulation with oscillatory currents to be variable over time (Veniero et al., 2015). Our functional connectivity analyses were done with average measures across 8 min periods; therefore, dynamic fluctuations in functional connectivity due to tACS below that time window are not evaluated. Another factor to take into account when examining tACS effects is the inter-subject variability

(in terms of anatomy, RSN spatial distributions and brain stimulation response), which might contribute to different tACS effects (Opitz et al., 2015a; Mennes et al., 2011; Mueller et al., 2013; Cohen et al., 2008). Future studies could expand on the use of subject-specific electric field simulations and RSNs to investigate the influence of individual differences on tACS effects.

Conclusions

In the present study we evaluated the effect of tACS on spontaneous low frequency BOLD signal fluctuations by applying tACS over the posterior cortex of healthy subjects at three different frequencies and with two different electrode montages. We offer a detailed description of the impact of tACS on spontaneous activity during and after stimulation. Stimulation frequency-dependent effects were given by opposite effects induced by 10 Hz (alpha) and 40 Hz (gamma). Most tACS effects were observed as modulation of inter-network functional connectivity (e.g., l-FP to the visual network), while intra-network functional connectivity changes were modest and only observed in the DAN, motor and visual networks. The left fronto-parietal control network showed the most extensive frequency-dependent modulation in functional connectivity, mainly with occipito-parietal areas. Our results suggest that tACS effects are not limited to regions below the electrodes but are influenced by network interactions, which should be taken into account when using tACS for studying brain function and behavior in health and disease.

Acknowledgements

We thank Ilona Pfahlert and Britta Perl for technical assistance during functional imaging experiments, Severin Heumüller and Hendrik Eichenauer for computer support, and Carsten Schmidt-Samoa for advice on statistical analysis. This work was supported by the Hermann and Lilly Schilling Foundation (to M. W.) and the European Neuroscience Campus Network, an Erasmus Mundus Joint Doctoral Program (to M.W. and K.W.).

Appendix A. Supplementary data

Supplementary data to this article can be found online at http://dx.doi.org/10.1016/j.neuroimage.2016.07.005.

References

Alekseichuk, I., Diers, K., Paulus, W., Antal, A., 2015. Transcranial electrical stimulation of the occipital cortex during visual perception modifies the magnitude of BOLD activity: a combined tES-fMRI approach. NeuroImage. http://dx.doi.org/10.1016/j.neuroimage.2015.11.034 (PubMed PMID: 26608246).

Ali, M.M., Sellers, K.K., Frohlich, F., 2013. Transcranial alternating current stimulation modulates large-scale cortical network activity by network resonance. J. Neurosci. 33 (27), 11262–11275. http://dx.doi.org/10.1523/JNEUROSCI.5867-12.2013 (PubMed PMID: 23825429).

Amadi, U., Ilie, A., Johansen-Berg, H., Stagg, C.J., 2013. Polarity-specific effects of motor transcranial direct current stimulation on fMRI resting state networks. NeuroImage 88C, 155–161. http://dx.doi.org/10.1016/j.neuroimage.2013.11.037 (PubMed PMID: 24287440; PubMed Central PMCID: PMCPMC3991849).

Antal, A., Bikson, M., Datta, A., Lafon, B., Dechent, P., Parra, L.C., et al., 2014. Imaging artifacts induced by electrical stimulation during conventional fMRI of the brain. NeuroImage 85 (Pt 3), 1040–1047. http://dx.doi.org/10.1016/j.neuroimage.2012.10.026 (PubMed PMID: 23099102; PubMed Central PMCID: PMC3759658).

Beckmann, C.F., DeLuca, M., Devlin, J.T., Smith, S.M., 2005. Investigations into resting-state connectivity using independent component analysis. Philos. Trans. R. Soc. Lond. Ser. B Biol. Sci. 360 (1457), 1001–1013. http://dx.doi.org/10.1098/rstb.2005.1634 (PubMed PMID: 16087444; PubMed Central PMCID: PMCPMC1854918).

Biswal, B., Yetkin, F.Z., Haughton, V.M., Hyde, J.S., 1995. Functional connectivity in the motor cortex of resting human brain using echo-planar MRI. Magn. Reson. Med. 34 (4), 537–541 (PubMed PMID: 8524021).

Brignani, D., Ruzzoli, M., Mauri, P., Miniussi, C., 2013. Is transcranial alternating current stimulation effective in modulating brain oscillations? PLoS One 8 (2), e56589. http://dx.doi.org/10.1371/journal.pone.0056589 (PubMed PMID: 23457586; PubMed Central PMCID: PMC3573000).

Brittain, J.S., Probert-Smith, P., Aziz, T.Z., Brown, P., 2013. Tremor suppression by rhythmic transcranial current stimulation. Curr. Biol. 23 (5), 436–440. http://dx.doi.org/10.1016/j.cub.2013.01.068 (PubMed PMID: 23416101; PubMed Central PMCID: PMC3629558).

Cabral-Calderin, Y., Anne Weinrich, C., Schmidt-Samoa, C., Poland, E., Dechent, P., Bahr, M., et al., 2016. Transcranial alternating current stimulation affects the BOLD signal in a frequency and task-dependent manner. Hum. Brain Mapp. 37 (1), 94–121. http://dx.doi.org/10.1002/hbm.23016 (PubMed PMID: 26503692).

Cabral-Calderin, Y., Schmidt-Samoa, C., Wilke, M., 2015. Rhythmic gamma stimulation affects bistable perception. J. Cogn. Neurosci. 27 (7), 1298–1307. http://dx.doi.org/10.1162/jocn_a_00781 (PubMed PMID: 25603029).

Canolty, R.T., Knight, R.T., 2010. The functional role of cross-frequency coupling. Trends Cogn. Sci. 14 (11), 506–515. http://dx.doi.org/10.1016/j.tics.2010.09.001 (PubMed PMID: 20932795; PubMed Central PMCID: PMCPMC3359652).

Chang, C., Glover, G.H., 2010. Time-frequency dynamics of resting-state brain connectivity measured with fMRI. NeuroImage 50 (1), 81–98. http://dx.doi.org/10.1016/j.neuroimage.2009.12.011 (PubMed PMID: 20006716; PubMed Central PMCID: PMCPMC2827259).

Cohen, A.L., Fair, D.A., Dosenbach, N.U., Miezin, F.M., Dierker, D., Van Essen, D.C., et al., 2008. Defining functional areas in individual human brains using resting functional connectivity MRI. NeuroImage 41 (1), 45–57. http://dx.doi.org/10.1016/j.neuroimage.2008.01.066 (PubMed PMID: 18367410; PubMed Central PMCID: PMC2705206).

Corbetta, M., Shulman, G.L., 2002. Control of goal-directed and stimulus-driven attention in the brain. Nat. Rev. Neurosci. 3 (3), 201–215. http://dx.doi.org/10.1038/nrn755 (PubMed PMID: 11994752).

Cox, R.W., 1996. AFNI: software for analysis and visualization of functional magnetic resonance neuroimages. Comput. Biomed. Res. 29 (3), 162–173 (PubMed PMID: 8812068).

Ehm, W., Bach, M., Kornmeier, J., 2011. Ambiguous figures and binding: EEG frequency modulations during multistable perception. Psychophysiology 48 (4), 547–558. http://dx.doi.org/10.1111/j.1469-8986.2010.01087.x (Epub 2010/08/28. PubMed PMID: 20796247).

Ekstrom, L.B., Roelfsema, P.R., Arsenault, J.T., Bonmassar, G., Vanduffel, W., 2008. Bottom-up dependent gating of frontal signals in early visual cortex. Science 321 (5887), 414–417. http://dx.doi.org/10.1126/science.1153276 (PubMed PMID: 18635806; PubMed Central PMCID: PMC3011100).

Fedorov, A., Chibisova, Y., Szymaszek, A., Alexandrov, M., Gall, C., Sabel, B.A., 2010. Non-invasive alternating current stimulation induces recovery from stroke. Restor. Neurol. Neurosci. 28 (6), 825–833. http://dx.doi.org/10.3233/RNN-2010-0580 (PubMed PMID: 21209497).

Feurra, M., Bianco, G., Santarnecchi, E., Del Testa, M., Rossi, A., Rossi, S., 2011b. Frequency-dependent tuning of the human motor system induced by transcranial oscillatory potentials. J. Neurosci. 31 (34), 12165–12170. http://dx.doi.org/10.1523/JNEUROSCI.0978-11.2011 (PubMed PMID: 21865459).

Feurra, M., Pasqualetti, P., Bianco, G., Santarnecchi, E., Rossi, A., Rossi, S., 2013. State-dependent effects of transcranial oscillatory currents on the motor system: what you think matters. J. Neurosci. 33 (44), 17483–17489. http://dx.doi.org/10.1523/JNEUROSCI.1414-13.2013 (PubMed PMID: 24174681).

Feurra, M., Paulus, W., Walsh, V., Kanai, R., 2011a. Frequency specific modulation of human somatosensory cortex. Front. Psychol. 2, 13. http://dx.doi.org/10.3389/fpsyg.2011.00013 (Epub 2011/06/30. PubMed PMID: 21713181; PubMed Central PMCID: PMC3111335).

Fox, M.D., Raichle, M.E., 2007. Spontaneous fluctuations in brain activity observed with functional magnetic resonance imaging. Nat. Rev. Neurosci. 8 (9), 700–711. http://dx.doi.org/10.1038/nrn2201 (PubMed PMID: 17704812).

Fox, M.D., Buckner, R.L., Liu, H., Chakravarty, M.M., Lozano, A.M., Pascual-Leone, A., 2014. Resting-state networks link invasive and noninvasive brain stimulation across diverse psychiatric and neurological diseases. Proc. Natl. Acad. Sci. U. S. A. 111 (41), E4367–E4375. http://dx.doi.org/10.1073/pnas.1405003111 (PubMed PMID: 25267639; PubMed Central PMCID: PMC4205651).

Fox, M.D., Halko, M.A., Eldaief, M.C., Pascual-Leone, A., 2012. Measuring and manipulating brain connectivity with resting state functional connectivity magnetic resonance imaging (fcMRI) and transcranial magnetic stimulation (TMS). NeuroImage 62 (4), 2232–2243. http://dx.doi.org/10.1016/j.neuroimage.2012.03.035 (PubMed PMID: 22465297; PubMed Central PMCID: PMC3518426).

Fox, M.D., Snyder, A.Z., Vincent, J.L., Corbetta, M., Van Essen, D.C., Raichle, M.E., 2005. The human brain is intrinsically organized into dynamic, anticorrelated functional networks. Proc. Natl. Acad. Sci. U. S. A. 102 (27), 9673–9678. http://dx.doi.org/10.1073/pnas.0504136102 (PubMed PMID: 15976020; PubMed Central PMCID: PMC1157105).

Gao, W., Lin, W., 2012. Frontal parietal control network regulates the anti-correlated default and dorsal attention networks. Hum. Brain Mapp. 33 (1), 192–202 (10.1002/hbm.21204. PubMed PMID: 21391263; PubMed Central PMCID: PMCPMC3131466).

Gratton, C., Lee, T.G., Nomura, E.M., D'Esposito, M., 2013. The effect of theta-burst TMS on cognitive control networks measured with resting state fMRI. Front. Syst. Neurosci. 7, 124. http://dx.doi.org/10.3389/fnsys.2013.00124 (PubMed PMID: 24416003; PubMed Central PMCID: PMC3874542).

Helfrich, R.F., Knepper, H., Nolte, G., Struber, D., Rach, S., Herrmann, C.S., et al., 2014b. Selective modulation of interhemispheric functional connectivity by HD-tACS shapes perception. PLoS Biol. 12 (12), e1002031. http://dx.doi.org/10.1371/journal.pbio.1002031 (PubMed PMID: 25549264; PubMed Central PMCID: PMC4280108).

Helfrich, R.F., Schneider, T.R., Rach, S., Trautmann-Lengsfeld, S.A., Engel, A.K., Herrmann, C.S., 2014a. Entrainment of brain oscillations by transcranial alternating current stimulation. Curr. Biol. 24 (3), 333–339. http://dx.doi.org/10.1016/j.cub.2013.12.041 (PubMed PMID: 24461998).

Helfrich, R.F., Herrmann, C.S., Engel, A.K., Schneider, T.R., 2015. Different coupling modes mediate cortical cross-frequency interactions. NeuroImage. http://dx.doi.org/10.1016/j.neuroimage.2015.11.035 (PubMed PMID: 26608244).

Hutchison, R.M., Womelsdorf, T., Gati, J.S., Everling, S., Menon, R.S., 2013. Resting-state networks show dynamic functional connectivity in awake humans and anesthetized macaques. Hum. Brain Mapp. 34 (9), 2154–2177. http://dx.doi.org/10.1002/hbm.22058 (PubMed PMID: 22438275).

Jenkinson, M., Beckmann, C.F., Behrens, T.E., Woolrich, M.W., Smith, S.M., 2012. Fsl. NeuroImage 62 (2), 782–790. http://dx.doi.org/10.1016/j.neuroimage.2011.09.015 (PubMed PMID: 21979382).

Jensen, O., Mazaheri, A., 2010. Shaping functional architecture by oscillatory alpha activity: gating by inhibition. Front. Hum. Neurosci. 4, 186. http://dx.doi.org/10.3389/fnhum.2010.00186 (PubMed PMID: 21119777; PubMed Central PMCID: PMC2990626).

Jensen, O., Bonnefond, M., Marshall, T.R., Tiesinga, P., 2015. Oscillatory mechanisms of feedforward and feedback visual processing. Trends Neurosci. 38 (4), 192–194. http://dx.doi.org/10.1016/j.tins.2015.02.006 (PubMed PMID: 25765320).

Joundi, R.A., Jenkinson, N., Brittain, J.S., Aziz, T.Z., Brown, P., 2012. Driving oscillatory activity in the human cortex enhances motor performance. Curr. Biol. 22 (5), 403–407. http://dx.doi.org/10.1016/j.cub.2012.01.024 (Epub 2012/02/07. PubMed PMID: 22305755; PubMed Central PMCID: PMC3343257).

Kanai, R., Chaieb, L., Antal, A., Walsh, V., Paulus, W., 2008. Frequency-dependent electrical stimulation of the visual cortex. Curr. Biol. 18 (23), 1839–1843. http://dx.doi.org/10.1016/j.cub.2008.10.027 (Epub 2008/11/26. PubMed PMID: 19026538).

Kar, K., Krekelberg, B., 2012. Transcranial electrical stimulation over visual cortex evokes phosphenes with a retinal origin. J. Neurophysiol. 108 (8), 2173–2178. http://dx.doi.org/10.1152/jn.00505.2012 (PubMed PMID: 22855777; PubMed Central PMCID: PMC3545027).

Kar, K., Krekelberg, B., 2014. Transcranial alternating current stimulation attenuates visual motion adaptation. J. Neurosci. 34 (21), 7334–7340. http://dx.doi.org/10.1523/JNEUROSCI.5248-13.2014 (PubMed PMID: 24849365; PubMed Central PMCID: PMCPMC4028503).

Laakso, I., Tanaka, S., Koyama, S., De Santis, V., Hirata, A., 2015. Inter-subject variability in electric fields of motor cortical tDCS. Brain Stimul. 8 (5), 906–913. http://dx.doi.org/10.1016/j.brs.2015.05.002 (PubMed PMID: 26026283).

Laczo, B., Antal, A., Niebergall, R., Treue, S., Paulus, W., 2012. Transcranial alternating stimulation in a high gamma frequency range applied over V1 improves contrast perception but does not modulate spatial attention. Brain Stimul. 5 (4), 484–491. http://dx.doi.org/10.1016/j.brs.2011.08.008 (Epub 2011/10/04. PubMed PMID: 21962982).

Lowe, M.J., Mock, B.J., Sorenson, J.A., 1998. Functional connectivity in single and multislice echoplanar imaging using resting-state fluctuations. NeuroImage 7 (2), 119–132. http://dx.doi.org/10.1006/nimg.1997.0315 (PubMed PMID: 9558644).

Mantini, D., Perrucci, M.G., Del Gratta, C., Romani, G.L., Corbetta, M., 2007. Electrophysiological signatures of resting state networks in the human brain. Proc. Natl. Acad. Sci. U. S. A. 104 (32), 13170–13175. http://dx.doi.org/10.1073/pnas.0700668104 (PubMed PMID: 17670949; PubMed Central PMCID: PMC1941820).

Mennes, M., Zuo, X.N., Kelly, C., Di Martino, A., Zang, Y.F., Biswal, B., et al., 2011. Linking inter-individual differences in neural activation and behavior to intrinsic brain dynamics. NeuroImage 54 (4), 2950–2959. http://dx.doi.org/10.1016/j.neuroimage.2010.10.046 (PubMed PMID: 20974260; PubMed Central PMCID: PMC3091620).

Mo, J., Liu, Y., Huang, H., Ding, M., 2013. Coupling between visual alpha oscillations and default mode activity. NeuroImage 68, 112–118. http://dx.doi.org/10.1016/j.neuroimage.2012.11.058 (PubMed PMID: 23228510; PubMed Central PMCID: PMC3557590).

Moeller, S., Yacoub, E., Olman, C.A., Auerbach, E., Strupp, J., Harel, N., et al., 2010. Multiband multislice GE-EPI at 7 tesla, with 16-fold acceleration using partial parallel imaging with application to high spatial and temporal whole-brain fMRI. Magn. Reson. Med. 63 (5), 1144–1153. http://dx.doi.org/10.1002/mrm.22361 (PubMed PMID: 20432285; PubMed Central PMCID: PMC2906244).

Mueller, S., Wang, D., Fox, M.D., Yeo, B.T., Sepulcre, J., Sabuncu, M.R., et al., 2013. Individual variability in functional connectivity architecture of the human brain. Neuron 77 (3), 586–595. http://dx.doi.org/10.1016/j.neuron.2012.12.028 (PubMed PMID: 23395382; PubMed Central PMCID: PMC3746075).

Murphy, K., Birn, R.M., Bandettini, P.A., 2013. Resting-state fMRI confounds and cleanup. NeuroImage 80, 349–359. http://dx.doi.org/10.1016/j.neuroimage.2013.04.001 (PubMed PMID: 23571418; PubMed Central PMCID: PMCPMC3720818).

Muthukumaraswamy, S.D., Singh, K.D., 2009. Functional decoupling of BOLD and gamma-band amplitudes in human primary visual cortex. Hum. Brain Mapp. 30 (7), 2000–2007. http://dx.doi.org/10.1002/hbm.20644 (PubMed PMID: 18729078).

Naghavi, H.R., Nyberg, L., 2005. Common fronto-parietal activity in attention, memory, and consciousness: shared demands on integration? Conscious. Cogn. 14 (2), 390–425. http://dx.doi.org/10.1016/j.concog.2004.10.003 (PubMed PMID: 15950889).

Nettekoven, C., Volz, L.J., Leimbach, M., Pool, E.M., Rehme, A.K., Eickhoff, S.B., et al., 2015. Inter-individual variability in cortical excitability and motor network connectivity following multiple blocks of rTMS. NeuroImage 118, 209–218. http://dx.doi.org/10.1016/j.neuroimage.2015.06.004 (PubMed PMID: 26052083).

Neuling, T., Rach, S., Herrmann, C.S., 2013. Orchestrating neuronal networks: sustained after-effects of transcranial alternating current stimulation depend upon brain states. Front. Hum. Neurosci. 7, 161. http://dx.doi.org/10.3389/fnhum.2013.00161 (PubMed PMID: 23641206; PubMed Central PMCID: PMC3639376).

Neuling, T., Ruhnau, P., Fusca, M., Demarchi, G., Herrmann, C.S., Weisz, N., 2015. Friends, not foes: magnetoencephalography as a tool to uncover brain dynamics during transcranial alternating current stimulation. NeuroImage 118, 406–413. http://dx.doi.org/10.1016/j.neuroimage.2015.06.026 (PubMed PMID: 26080310; PubMed Central PMCID: PMC4686537).

Neuling, T., Wagner, S., Wolters, C.H., Zaehle, T., Herrmann, C.S., 2012. Finite-element model predicts current density distribution for clinical applications of tDCS and tACS. Front. Psychiatr. 3, 83. http://dx.doi.org/10.3389/fpsyt.2012.00083 (PubMed PMID: 23015792; PubMed Central PMCID: PMC3449241).

Opitz, A., Fox, M.D., Craddock, R.C., Colcombe, S., Milham, M.P., 2015a. An integrated framework for targeting functional networks via transcranial magnetic stimulation. NeuroImage 127, 86–96. http://dx.doi.org/10.1016/j.neuroimage.2015.11.040 (PubMed PMID: 26608241).

Opitz, A., Paulus, W., Will, S., Antunes, A., Thielscher, A., 2015b. Determinants of the electric field during transcranial direct current stimulation. NeuroImage 109, 140–150. http://dx.doi.org/10.1016/j.neuroimage.2015.01.033 (PubMed PMID: 25613437).

Ozen, S., Sirota, A., Belluscio, M.A., Anastassiou, C.A., Stark, E., Koch, C., et al., 2010. Transcranial electric stimulation entrains cortical neuronal populations in rats. J. Neurosci. 30 (34), 11476–11485. http://dx.doi.org/10.1523/JNEUROSCI.5252-09.2010 (PubMed PMID: 20739569; PubMed Central PMCID: PMC2937280).

Park, H.J., Friston, K., 2013. Structural and functional brain networks: from connections to cognition. Science 342 (6158), 1238411. http://dx.doi.org/10.1126/science.1238411 (PubMed PMID: 24179229).

Parkes, L.M., Fries, P., Kerskens, C.M., Norris, D.G., 2004. Reduced BOLD response to periodic visual stimulation. NeuroImage 21 (1), 236–243 (PubMed PMID: 14741661).

Peraza, L.R., Taylor, J.P., Kaiser, M., 2015. Divergent brain functional network alterations in dementia with Lewy bodies and Alzheimer's disease. Neurobiol. Aging 36 (9), 2458–2467. http://dx.doi.org/10.1016/j.neurobiolaging.2015.05.015 (PubMed PMID: 26115566).

Polania, R., Nitsche, M.A., Korman, C., Batsikadze, G., Paulus, W., 2012. The importance of timing in segregated theta phase-coupling for cognitive performance. Curr. Biol. 22 (14), 1314–1318. http://dx.doi.org/10.1016/j.cub.2012.05.021 (Epub 2012/06/12. PubMed PMID: 22683259).

Raco, V., Bauer, R., Olenik, M., Brkic, D., Gharabaghi, A., 2014. Neurosensory effects of transcranial alternating current stimulation. Brain Stimul. 7 (6), 823–831. http://dx.doi.org/10.1016/j.brs.2014.08.005 (PubMed PMID: 25442154).

Raichle, M.E., 2010. Two views of brain function. Trends Cogn. Sci. 14 (4), 180–190. http://dx.doi.org/10.1016/j.tics.2010.01.008 (PubMed PMID: 20206576).

Raichle, M.E., 2015. The restless brain: how intrinsic activity organizes brain function. Philos. Trans. R. Soc. Lond. Ser. B Biol. Sci. 370 (1668). http://dx.doi.org/10.1098/rstb.2014.0172 (PubMed PMID: 25823869; PubMed Central PMCID: PMCPMC4387513).

Raichle, M.E., MacLeod, A.M., Snyder, A.Z., Powers, W.J., Gusnard, D.A., Shulman, G.L., 2001. A default mode of brain function. Proc. Natl. Acad. Sci. U. S. A. 98 (2), 676–682. http://dx.doi.org/10.1073/pnas.98.2.676 (PubMed PMID: 11209064; PubMed Central PMCID: PMCPMC14647).

Reato, D., Rahman, A., Bikson, M., Parra, L.C., 2013. Effects of weak transcranial alternating current stimulation on brain activity — a review of known mechanisms from animal studies. Front. Hum. Neurosci. 7, 687. http://dx.doi.org/10.3389/fnhum.2013.00687 (PubMed PMID: 24167483; PubMed Central PMCID: PMC3805939).

Salomons, T.V., Dunlop, K., Kennedy, S.H., Flint, A., Geraci, J., Giacobbe, P., et al., 2014. Resting-state cortico-thalamic-striatal connectivity predicts response to dorsomedial prefrontal rTMS in major depressive disorder. Neuropsychopharmacology 39 (2), 488–498. http://dx.doi.org/10.1038/npp.2013.222 (PubMed PMID: 24150516; PubMed Central PMCID: PMCPMC3870791).

Santarnecchi, E., Polizzotto, N.R., Godone, M., Giovannelli, F., Feurra, M., Matzen, L., et al., 2013. Frequency-dependent enhancement of fluid intelligence induced by transcranial oscillatory potentials. Curr. Biol. 23 (15), 1449–1453. http://dx.doi.org/10.1016/j.cub.2013.06.022 (PubMed PMID: 23891115).

Scheeringa, R., Petersson, K.M., Kleinschmidt, A., Jensen, O., Bastiaansen, M.C., 2012. EEG alpha power modulation of fMRI resting-state connectivity. Brain Connect. 2 (5), 254–264. http://dx.doi.org/10.1089/brain.2012.0088 (PubMed PMID: 22938826; PubMed Central PMCID: PMC3621304).

Schutter, D.J., 2015. Cutaneous retinal activation and neural entrainment in transcranial alternating current stimulation: a systematic review. NeuroImage. http://dx.doi.org/10.1016/j.neuroimage.2015.09.067 (PubMed PMID: 26453929).

Setsompop, K., Gagoski, B.A., Polimeni, J.R., Witzel, T., Wedeen, V.J., Wald, L.L., 2012. Blipped-controlled aliasing in parallel imaging for simultaneous multislice echo planar imaging with reduced g-factor penalty. Magn. Reson. Med. 67 (5), 1210–1224. http://dx.doi.org/10.1002/mrm.23097 (PubMed PMID: 21858868; PubMed Central PMCID: PMC3323676).

Shmuel, A., Leopold, D.A., 2008. Neuronal correlates of spontaneous fluctuations in fMRI signals in monkey visual cortex: implications for functional connectivity at rest. Hum. Brain Mapp. 29 (7), 751–761. http://dx.doi.org/10.1002/hbm.20580 (PubMed PMID: 18465799).

Spaak, E., Bonnefond, M., Maier, A., Leopold, D.A., Jensen, O., 2012. Layer-specific entrainment of gamma-band neural activity by the alpha rhythm in monkey visual cortex. Curr. Biol. 22 (24), 2313–2318. http://dx.doi.org/10.1016/j.cub.2012.10.020 (PubMed PMID: 23159599; PubMed Central PMCID: PMCPMC3528834).

Spreng, R.N., Sepulcre, J., Turner, G.R., Stevens, W.D., Schacter, D.L., 2013. Intrinsic architecture underlying the relations among the default, dorsal attention, and frontoparietal control networks of the human brain. J. Cogn. Neurosci. 25 (1), 74–86. http://dx.doi.org/10.1162/jocn_a_00281 (PubMed PMID: 22905821; PubMed Central PMCID: PMCPMC3816715).

Struber, D., Rach, S., Neuling, T., Herrmann, C.S., 2015. On the possible role of stimulation duration for after-effects of transcranial alternating current stimulation. Front. Cell. Neurosci. 9, 311. http://dx.doi.org/10.3389/fncel.2015.00311 (PubMed PMID: 26321912; PubMed Central PMCID: PMC4530587).

Struber, D., Rach, S., Trautmann-Lengsfeld, S.A., Engel, A.K., Herrmann, C.S., 2014. Antiphasic 40 Hz oscillatory current stimulation affects bistable motion perception. Brain Topogr. 27 (1), 158–171. http://dx.doi.org/10.1007/s10548-013-0294-x (PubMed PMID: 23709044).

Tagliazucchi, E., von Wegner, F., Morzelewski, A., Brodbeck, V., Laufs, H., 2012. Dynamic BOLD functional connectivity in humans and its electrophysiological correlates. Front. Hum. Neurosci. 6, 339. http://dx.doi.org/10.3389/fnhum.2012.00339 (PubMed PMID: 23293596; PubMed Central PMCID: PMC3531919).

Thielscher, A., Antunes, A., Saturnino, G.B., 2015. Field modeling for transcranial magnetic stimulation: a useful tool to understand the physiological effects of TMS? Conference Proceedings : Annual International Conference of the IEEE Engineering in Medicine and Biology Society IEEE Engineering in Medicine and Biology Society Annual Conference Vol. 2015, pp. 222–225. http://dx.doi.org/10.1109/EMBC.2015.7318340 (PubMed PMID: 26736240)

Thielscher, A., Opitz, A., Windhoff, M., 2011. Impact of the gyral geometry on the electric field induced by transcranial magnetic stimulation. NeuroImage 54 (1), 234–243. http://dx.doi.org/10.1016/j.neuroimage.2010.07.061 (PubMed PMID: 20682353).

Tomasi, D., Wang, G.J., Volkow, N.D., 2013. Energetic cost of brain functional connectivity. Proc. Natl. Acad. Sci. U. S. A. 110 (33), 13642–13647. http://dx.doi.org/10.1073/pnas.1303346110 (PubMed PMID: 23898179; PubMed Central PMCID: PMC3746878).

Turi, Z., Ambrus, G.G., Janacsek, K., Emmert, K., Hahn, L., Paulus, W., et al., 2013. Both the cutaneous sensation and phosphene perception are modulated in a frequency-specific manner during transcranial alternating current stimulation. Restor. Neurol. Neurosci. 31 (3), 275–285. http://dx.doi.org/10.3233/RNN-120297 (PubMed PMID: 23478342).

Van Dijk, K.R., Hedden, T., Venkataraman, A., Evans, K.C., Lazar, S.W., Buckner, R.L., 2010. Intrinsic functional connectivity as a tool for human connectomics: theory, properties, and optimization. J. Neurophysiol. 103 (1), 297–321. http://dx.doi.org/10.1152/jn.00783.2009 (PubMed PMID: 19889849; PubMed Central PMCID: PMC2807224).

Veniero, D., Vossen, A., Gross, J., Thut, G., 2015. Lasting EEG/MEG aftereffects of rhythmic transcranial brain stimulation: level of control over oscillatory network activity. Front. Cell. Neurosci. 9, 477. http://dx.doi.org/10.3389/fncel.2015.00477 (PubMed PMID: 26696834; PubMed Central PMCID: PMC4678227).

Vincent, J.L., Kahn, I., Snyder, A.Z., Raichle, M.E., Buckner, R.L., 2008. Evidence for a frontoparietal control system revealed by intrinsic functional connectivity. J. Neurophysiol. 100 (6), 3328–3342. http://dx.doi.org/10.1152/jn.90355.2008 (PubMed PMID: 18799601; PubMed Central PMCID: PMCPMC2604839).

von Stein, A., Sarnthein, J., 2000. Different frequencies for different scales of cortical integration: from local gamma to long range alpha/theta synchronization. Int. J. Psychophysiol. 38 (3), 301–313 (PubMed PMID: 11102669).

Vossen, A., Gross, J., Thut, G., 2015. Alpha power increase after transcranial alternating current stimulation at alpha frequency (alpha-tACS) reflects plastic changes rather than entrainment. Brain Stimul. 8 (3), 499–508. http://dx.doi.org/10.1016/j.brs.2014.12.004 (PubMed PMID: 25648377; PubMed Central PMCID: PMC4464304).

Vosskuhl, J., Huster, R.J., Herrmann, C.S., 2015. BOLD signal effects of transcranial alternating current stimulation (tACS) in the alpha range: a concurrent tACS-fMRI study. NeuroImage. http://dx.doi.org/10.1016/j.neuroimage.2015.10.003 (PubMed PMID: 26458516).

Wach, C., Krause, V., Moliadze, V., Paulus, W., Schnitzler, A., Pollok, B., 2013. Effects of 10 Hz and 20 Hz transcranial alternating current stimulation (tACS) on motor functions and motor cortical excitability. Behav. Brain Res. 241, 1–6. http://dx.doi.org/10.1016/j.bbr.2012.11.038 (PubMed PMID: 23219965).

Wang, J., Yang, Y., Fan, L., Xu, J., Li, C., Liu, Y., et al., 2015. Convergent functional architecture of the superior parietal lobule unraveled with multimodal neuroimaging approaches. Hum. Brain Mapp. 36 (1), 238–257. http://dx.doi.org/10.1002/hbm.22626 (PubMed PMID: 25181023; PubMed Central PMCID: PMC4268275).

Windhoff, M., Opitz, A., Thielscher, A., 2013. Electric field calculations in brain stimulation based on finite elements: an optimized processing pipeline for the generation and usage of accurate individual head models. Hum. Brain Mapp. 34 (4), 923–935. http://dx.doi.org/10.1002/hbm.21479 (PubMed PMID: 22109746).

Witkowski, M., Garcia-Cossio, E., Chander, B.S., Braun, C., Birbaumer, N., Robinson, S.E., et al., 2015. Mapping entrained brain oscillations during transcranial alternating current stimulation (tACS). NeuroImage http://dx.doi.org/10.1016/j.neuroimage.2015.10.024 (PubMed PMID: 26481671).

Xu, J., Moeller, S., Auerbach, E.J., Strupp, J., Smith, S.M., Feinberg, D.A., et al., 2013. Evaluation of slice accelerations using multiband echo planar imaging at 3 T. NeuroImage 83, 991–1001. http://dx.doi.org/10.1016/j.neuroimage.2013.07.055 (PubMed PMID: 23899722; PubMed Central PMCID: PMC3815955).

Zaehle, T., Rach, S., Herrmann, C.S., 2010. Transcranial alternating current stimulation enhances individual alpha activity in human EEG. PLoS One 5 (11), e13766. http://dx.doi.org/10.1371/journal.pone.0013766 (PubMed PMID: 21072168; PubMed Central PMCID: PMC2967471).

Zang, Y.F., He, Y., Zhu, C.Z., Cao, Q.J., Sui, M.Q., Liang, M., et al., 2007. Altered baseline brain activity in children with ADHD revealed by resting-state functional MRI. Brain and Development 29 (2), 83–91. http://dx.doi.org/10.1016/j.braindev.2006.07.002 (PubMed PMID: 16919409).

Zhan, Z., Xu, L., Zuo, T., Xie, D., Zhang, J., Yao, L., et al., 2014. The contribution of different frequency bands of fMRI data to the correlation with EEG alpha rhythm. Brain Res. 1543, 235–243. http://dx.doi.org/10.1016/j.brainres.2013.11.016 (PubMed PMID: 24275197).

Zhu, D., Chang, J., Freeman, S., Tan, Z., Xiao, J., Gao, Y., et al., 2014. Changes of functional connectivity in the left frontoparietal network following aphasic stroke. Front. Behav. Neurosci. 8, 167. http://dx.doi.org/10.3389/fnbeh.2014.00167 (PubMed PMID: 24860452; PubMed Central PMCID: PMC4026698).

Zou, Q.H., Zhu, C.Z., Yang, Y., Zuo, X.N., Long, X.Y., Cao, Q.J., et al., 2008. An improved approach to detection of amplitude of low-frequency fluctuation (ALFF) for resting-state fMRI: fractional ALFF. J. Neurosci. Methods 172 (1), 137–141. http://dx.doi.org/10.1016/j.jneumeth.2008.04.012 (PubMed PMID: 18501969; PubMed Central PMCID: PMC3902859).

Zuo, X.N., Di Martino, A., Kelly, C., Shehzad, Z.E., Gee, D.G., Klein, D.F., et al., 2010. The oscillating brain: complex and reliable. NeuroImage 49 (2), 1432–1445. http://dx.doi.org/10.1016/j.neuroimage.2009.09.037 (PubMed PMID: 19782143; PubMed Central PMCID: PMC2856476).